Pal, D. C., Trumbull, R. B., Wiedenbeck, M. (2010): Chemical and boron isotope compositions of tourmaline from the Jaduguda U (-Cu-Fe) deposit, Singhbhum shear zone, India: implications for the source and evolution of the mineralizing fluid. - Chemical Geology, 277, 3-4, 245-260

DOI: 10.1016/j.chemgeo.2010.08.008

Chemical and boron isotope compositions of tourmaline from the Jaduguda U (-Cu-Fe) deposit, Singhbhum shear zone, India: implications for the sources and evolution of mineralizing fluids

Dipak C. Pal[1, 2*], Robert B. Trumbull[1], Michael Wiedenbeck[1]

1 GFZ German Research Centre for Geosciences, Telegrafenberg, 14473 Potsdam, Germany

2 Permanent address: Department of Geological Sciences, Jadavpur University, Kolkata 700 032 WB India; email: dipak.pal@gmail.com; dcpal@geology.jdvu.ac.in; Phone +91 33 2414 6666 Ext 2724; FAX: +91 33 2414 6781

[*] Corresponding author

Abstract

The Proterozoic Jaduguda U (-Cu-Fe) deposit in the Singhbhum shear zone, eastern India hosts the oldest and most productive uranium mine in India. The polymetallic ores in Jaduguda are hosted in altered, sheared and metamorphosed volcano-sedimentary rocks, and this complexity has lead to a confusion in ore genetic models for the deposit. A characteristic of the mineralization is the presence of abundant tourmaline, locally exceeding 50 vol%, which is spatially associated with U and Cu mineralization in all rock types and its chemical and B-isotopic variations provide important constraints on fluid source(s) and ore deposit affinity. We examined tourmaline from the U-Cu ore zone and adjacent footwall and hanging wall meta-sedimentary rocks.

Tourmaline grew in three different stages. Pre-kinematic Tourmaline-1, represented by fractured and porphyroblastic grains, is ubiquitous in the wall rocks and the U-Cu zone. Syn-kinematic Tourmaline-2 and post-kinematic Tourmaline-3 are found exclusively in the U-Cu zone, where intense shear deformation has focussed fluid flow, alteration and metamorphism. All tourmalines belong to the alkalic group and most are dravitic. Systematic contrasts in major element compositions between Tourmaline-1 and Tourmaline-2 are attributed to the influence of high fluid/rock ratios in the U-Cu ore zone.

Tourmaline from the Jaduguda deposit exhibits a wide overall range of $\delta^{11}B$ values from -6.8 to +17.2 ‰ . Positive values of Tourmaline-1 are irrespective of host rock and ore association (U or U + Cu), and range between +2.3 to +17.2 ‰ (n=44). The calculated $\delta^{11}B$ values of fluid in equilibrium with this tourmaline (for mineralization temperatures of 300-450°C) range from ~ +4 to ~ +20‰.The $\delta^{11}B$ values of syn-kinematic Tourmaline-2 are much lower than Tourmaline-1, between -6.8 and +4 ‰ (n=7) and the corresponding fluid $\delta^{11}B$ values are -4.8 +6‰.

The high values of $\delta^{11}B$ for Tourmaline-1 and early fluid suggest a marine evaporite or basinal brine was the source of boron, and this fits abundant mineralogical and geochemical evidence for highly-saline fluids during mineralization. We propose that the isotopically lighter fluid associated with Tourmaline-2 and related syn-kinematic mineralization/mobilization was derived from the metamorphic volcano-sedimentary rocks at high fluid/rock ratios in and around the shear zone. Post-kinematic Tourmaline-3 is compositionally and isotopically ($\delta^{11}B$ =+4 to +11.1 ‰, n=5) similar to

Tourmaline-1 in the same samples, suggesting it formed by by local recrystallization of the early tourmaline or from a renewed influx of saline fluids similar to those which formed the pre-kinematic mineralization. Integrating the results of this tourmaline study with the geological and geochemical characteristics of the Jaduguda U-(Cu-Fe) mineralization suggests that it is best regarded as a variant of the Fe-oxide (Cu-U-REE) or IOCG class of deposits.

Key words: tourmaline, boron isotope, SIMS, uranium, Singhbhum, India, IOCG

1 Introduction

The Singhbhum shear zone (SSZ), eastern India, is one of the most important Proterozoic polymetallic mineral belts in India (U and Cu as main commodities and magnetite, Ni, Au, Ag, Se, Te, Mo as by-products). Presently there are six uranium-producing mines (Turamdih, Banduhurang, Narwapahar, Bhatin, Jaduguda and Bagjata) located between Turamdih on the west and Bagjata on the east (Fig.1). The ores in these deposits are hosted by deformed and metamorphosed volcano-sedimentary rocks of Archaean and Paleoproterozoic age. The Singhbhum shear zone was the site of profuse K, Na, H^+ and B-metasomatism (Dunn and Dey, 1942; Banerji and Talapatra 1966; Talapatra, 1968; Ghosh, 1972; Banerjee, 1982; Sarkar, 1984, Bhattacharya et al., 1992; Sengupta et al., 2005, Pal et al., 2009), which is manifested in widespread and voluminous occurrences of feldspathic schist/"soda granite" (albite-oligoclase dominated rocks), biotite schist, chlorite schist and tourmalinite. Although most workers proposed a hydrothermal origin for these deposits, the source (s) of hydrothermal fluid (s) is uncertain. Proposed theories include magmatic fluid, evaporite-derived/basinal brine and seawater (Dunn and Dey, 1942; Sarkar, 1984; Changkakoti et al., 1987; Mishra and Singh, 2003; Mishra et al., 2003). Related to the uncertain fluid provenance in these deposits is the question of a workable metallogenetic model. Classic models have varied from magmatic-hydrothermal (Dunn and Dey, 1942) to metamorphogenic related to migmatization (Banerji 1962; Talapatra, 1968; Banerji, 1981). Other workers suggested an affinity to the volcanogenic massive sulphide deposits (VMS; Sarkar, 1984), and most recently, Pal et al. (2009) suggested the Singhbhum ore deposits are of the Fe-oxide (Cu-U-REE) (IOCG) type . Although most mineralization in the shear zone seems to predate deformation (Sarkar, 1984, Pandey et al., 1994, Pal et al., 2009), multiple events of mobilization and/or enrichment are indicated (Banerji, 1981; Rao and Rao, 1983; Pal et al., 2009). Accordingly any model on hydrothermal mineralization and its temporal evolution must take the multi- stage history of mineralization/mobilization into account.

The Jaduguda deposit, located at the central part of the mineralized belt, hosts the most productive uranium mine (Jaduguda mine) in India, which has produced uranium for about five decades. Tourmaline is a ubiquitous minor to major mineral, locally exceeding 50 vol%, in the rocks

that host uranium ± base metals mineralization in this deposit. Sengupta et al., (2005) documented the textures and chemical compositions of multi-stage tourmaline growth (pre-, syn- and post-tectonic) in the Singhbhum shear zone during the tectono-metamorphic evolution. They noted the association of tourmaline with mineralization at some of the sample localities but the emphasis of their study was on the metamorphic history. In this paper , we examine specifically the use of textures, chemical compositions and boron isotopic signatures ($\delta^{11}B$) of tourmaline in mineralized zones and wallrock to constrain the source and evolution of mineralizing fluid (s) and thus to better define a metallogenic model for the Jaduguda polymetallic deposit.

2 Geological background

2.1 General geology

The ~ 200 km long and ~ 1-5 km wide Singhbhum shear zone (Fig. 1) occurs close to the boundary between the Archaean Singhbhum cratonic nucleus (3.3-3.5 Ga; Moorbath et al., 1986; Saha et al., 1988; Saha, 1994; Sharma et al., 1994; Misra et al., 1999) on the south and the Proterozoic North Singhbhum Fold belt on the north (Fig. 1). Two prominent basins, namely the Iron ore basin (with Iron ore Group greenstone sequence; ~ 3.3-3.5 Ga; Augé et al., 2003; Mukhopadhyay et al., 2008) and the Dhanjori basin (with Dhanjori Group rocks; ~ 2.1 Ga or ~ 2.8 Ga? Roy et al., 2002, Misra and Johnson, 2005) occupies the northwestern and southeastern part of the cratonic nucleus, respectively (Fig. 1). Iron Ore Group (IOG), with banded iron formation, comprises metasedimentary rocks, metavolcanic rocks, and mafic sills and dikes. The Dhanjori Group is represented by vesicular basalts (locally pillowed), and komatiite with intercalated arkose, feldspathic arenite-litharenite/lithic wacke, and pelitic metasediments (Mazumder and Sarkar, 2004). This volcano-sedimentary sequence is intruded by gabbro-peridotite (Sarkar and Deb 1971; Banerjee, 1982; Gupta et al., 1985). Siliciclastic rocks of the fold belt (Singhbhum Group) overlie the Iron Ore Group and Dhanjori Group rocks. Analysis of the sedimentary structures, and sedimentary facies indicates that the entire volcano-sedimentary column of the North Singhbhum Fold Belt was likely deposited in an intracontinental rift basin in rapidly changing tectonic environment (Mazumder and Sarkar, 2004; Mazumder, 2005). The Dhanjori rocks are inferred to have been deposited mostly in alluvial (lower Dhanjori) and fluvial and partly in lacustrine (upper Dhanjori) settings under a semi-arid climate (Mazumder and Sarkar, 2004). The Singhbhum Group is inferred to have been deposited in a shallow to deep marine environment with later transition to mostly terrestrial (fluvial-aeolian) or shallow marine environment (Mazumder, 2005). The sedimentary facies that includes meta-conglomerate and meta-greywacke-arenite in the Jaduguda deposit was likely deposited in a fluvial fan environment (Virnave et al., 1994).

The Singhbhum brittle-ductile shear zone (SSZ), cuts across rocks of Iron ore Group, Dhanjori Group and the Singhbhum Group. The progressive deformation resulted prominent mylonitic foliation

and conspicuous down-dip lineation followed by folding of mylonitic foliation and development of tight isoclinal reclined folds which were superimposed in turn by upright gently plunging asymmetric folds with axial planar crenulation cleavage (Ghosh and Sengupta, 1987, 1990; Sengupta and Ghosh, 1997). Prograde metamorphism that culminated in epidote-amphibolite facies (480 ± 40˚C and 6.4 ± 0.4 kbar) accompanied the progressive deformation (Sengupta et al., 2005). The retrograde metamorphism exemplified by hydration of prograde assemblages postdated the progressive ductile deformation. Finally, multiple stages of brittle deformation followed the ductile shearing stage (Srivastava and Pradhan, 1995).

2.2 The Jaduguda deposit

The Jaduguda uranium deposit is located close to the boundary between the volcano-sedimentary rocks of Dhanjori Group and the siliciclastic rocks of the Singhbhum Group (Fig. 1 and Fig. 2). The rocks in and around the deposit are represented by amygdular metabasalt, biotite schist, chlorite schist, quartzite, meta-conglomerate, muscovite schist, and kyanite-bearing quartzite/sericite schist (Fig. 2). In the Jaduguda mine, strong deformation of the rocks has produced two sets of foliation both of which are parallel to bedding plane (Venkataraman et al., 1971). The stratabound ore bodies, dipping ~ 40^0→ NE/ENE, parallel the foliation planes and the ore shoots plunge parallel to down-dip lineation defined by elongate minerals, mineral aggregates, and stretched pebbles (Venkataraman et al., 1971).

Two mineable uranium lodes extend from surface with uniform persistence both along strike (~ 600m length) and dip (~ 900m depth). These two lodes, defined by recoverable grade of uranium, are commonly referred to as the 'Footwall Lode' or the southern lode and the 'Hangwall Lode' or the northern lode. Figure 3 shows the distribution of different rock types and the two uranium ore lodes along an idealised section in the 555 m level in Jaduguda mine. This general distribution pattern holds for the other levels as well, excepting variable widths of individual rock units. The footwall uranium lode is the most important in terms of grade and tonnage of uranium., Significant sulphide mineralization with recoverable Cu-, Ni- and Mo-sulphides also occurs at the footwall side of, and overlapping with, the footwall uranium lode. Sulphide minerals are sparse outside this zone. Uraninite is the main ore mineral of uranium with minor pitchblende, brannerite and autunite. Sulphide minerals are predominantly chalcopyrite and pyrite with variable proportions of pentlandite, millerite, and molybdenite. Generally, the uranium lodes and the accompanying zone of sulphide mineralization in the Jaduguda mine are very rich in tourmaline, locally exceeding 50 vol%. Tourmaline is also present outside these zones (*cf.* Sengupta et al., 2005), but in low concentration. The close association of large volumes of tourmaline with the mineralized zones (both U and base metals) and the presence of tourmaline in quartz-sulphide veins indicate a causal relation between boron metasomatism and U and Cu mineralization in Jaduguda.

3 Sample location and sample description

Tourmaline-bearing samples from in and around the footwall uranium lode in the 555 m working level comprise five rock types, namely quartz-tourmaline rock, quartz-sulphide vein, biotite schist, chlorite schist and meta-conglomerate (Fig. 3). For the purpose of this study, we classified the sample locations into three zones based on the ore mineral association (e.g. oxide with minor/no sulphide and oxide plus ubiquitous and abundant sulphide) and the relative positions with reference to the U-Cu zone. The sample locations are: a) the U-Cu zone represented by chlorite schist, biotite schist and quartz-sulphide veins, b) the footwall (footwall of U-Cu zone) U zone represented by quartz-tourmaline rock, and c) the hanging wall (hanging wall of U-Cu zone) U zone represented by meta-conglomerate (Fig. 3). The host rocks of the U-Cu zone are more strongly crushed and brecciated compared to the footwall and the hanging wall zone, resulting in friable assemblage (commonly referred to as "granular rock" by local miners). Uraninite occurs in all three of these zones, but prominent sulphide mineralization occurs only in the U-Cu zone.

The footwall quartz-tourmaline rock is intercalated with the footwall quartzite (Fig. 3). The rock is characterized by millimetre to centimetre-wide alternating quartz-rich and tourmaline-rich bands, and consists predominantly of fine-grained tourmaline (≤ ~ 200 μm), quartz and hematite-dusted feldspar with minor to accessory chlorite, titanite, monazite, ilmenite, brannerite and uraninite. Individual bands are stretched and locally boudinadged. Tourmaline grains and grain clusters commonly display sigmoidal fabric and pressure shadows implying a pre-kinematic growth with regard to the ductile shearing (Fig 4a). Most tourmaline grains are optically homogeneous, rarely with greenish blue rim on a dark brown/yellowish brown core. Uraninite occurs as inclusions in tourmaline and also as dissemination in the matrix. Sulphide minerals are scarce. The mineralogy of the banded quartz-tourmaline rock and its intimate association with quartzite suggests a sedimentary protolith.

The hanging wall meta-conglomerate (Fig. 3) comprises large ellipsoidal quartzite pebbles in a matrix of tourmaline, magnetite, apatite, chlorite, biotite, ilmenite, titanite, uraninite, and rare allanite. Like the quartz-tourmaline rock at the footwall, this meta-conglomerate contains minor sulphide minerals. The pebbles contain rounded grains of chromite (with ~ 52 wt% Cr_2O_3) that are commonly rimmed by ferritchromite (with ~ 17 wt% Cr_2O_3). Coarse (~ 500 μm) tourmaline grains locally contain tiny inclusions of magnetite, quartz and uraninite (Fig. 4b). As in the quartz-tourmaline rock, most tourmaline grains are deep brown/yellow and optically unzoned. The presence of well-rounded detrital chromite and pebbles indicate that this rock was derived from a sedimentary protolith.

Quartz sulphide veins (up to ~ 0.5 m wide), locally displaying isoclinal folding and therefore pre- or synkinematic, comprise predominantly large (2-3 centimetres) ribbon quartz veins, chlorite,

tourmaline, biotite and apatite. Chloritization of biotite is ubiquitous. Tourmaline in the quartz-sulphide vein is mostly optically heterogeneous (Fig. 4c, d), particularly where associated with chloritization of biotite. Irregular patchy brown/honey colored tourmaline is commonly rimmed or crosscut by greenish blue tourmaline.

The biotite schist sampled for this study occurs as relict pockets and lenses in chlorite schist. It comprises predominantly biotite (locally ~ 60-70 vol%), tourmaline and chlorite with minor/negligible quartz. Chloritization of biotite is locally associated with chalcopyrite. Tourmaline occurs in two textural modes in this rock type. Of the first type are greenish blue/brown grains (≤ ~ 500 μm), disseminated in the biotite groundmass, which commonly display complex optical zoning. Relatively light colored tourmaline occurs either as rims on inclusion-riddle deep-green/greenish blue core or along microcracks of darker deep green/brown tourmaline (Fig. 4e, f). These tourmaline grains are locally aligned parallel to foliation. The second type consists of light brown to honey yellow, optically homogeneous and very coarse (up to ~ 1 cm) tourmaline in clusters of radiating grains (Fig. 4g), which overprint foliation defined by biotite. Chalcopyrite specks and stringers are commonly intimately associated with this tourmaline. Strongly variable modal percentages of constituent minerals and the high content of Fe, Mg, Ti (Fe_2O_3, MgO and TiO_2 concentrations are ~ 22, 13, 1.5 wt% respectively; unpublished data) suggests that the biotite schist represents an altered and metamorphosed mafic protolith. Outside the shear zone, biotite schist displays gradational contacts with the Dhanjori basic volcanic rocks, occasionally with an intermediate stage of hornblende-biotite schist between (Sarkar and Deb, 1971). Although not observed in our samples, replacement of amphibole by biotite has been observed in Jaduguda (Das, 2009) and elsewhere in the mineral district (Ghosh, 1972). These features further support our contention that the biotite schist represents a mafic protolith.

Chlorite schist, comprising predominantly quartz and chlorite with variable proportions of biotite, tourmaline and apatite, is strongly heterogeneous in terms of modal abundances of the constituent minerals. Chloritization of biotite is ubiquitous and is commonly associated with chalcopyrite formation (*cf* Das, 2009). Tourmaline occurs in several textural forms. Tourmaline in quartz-rich zones is fine-grained (≤ ~ 200 μm) brown/honey colored and occurs as disseminated grains or in clusters paralleling foliation, similar to those in the quartz-tourmaline rock. Tourmaline in the chlorite rich domains, where chloritization of biotite is pervasive, are coarse-grained (~ 500 μm) and complexly optically zoned (Fig. 4h). Like in the quartz-sulphide vein, irregular patchy brown/honey colored tourmaline cores are commonly rimmed by greenish blue tourmaline, the latter also occurring in microcracks of the former. The variable modal percentage, ubiquitous chloritization of biotite and the occurrences of relict biotite-schist pockets in this rock imply that it was derived from the biotite schist and a mafic protolith. However, the quartz-rich variety of chlorite schist, with fine-grained tourmaline, like in quartz-tourmaline rock, may have been derived from a sedimentary protolith.

Based on the above observations and in line with a previous study on tourmaline from the Singhbhum shear zone by Sengupta et al. (2005) we distinguish three stages of tourmaline growth in the Jaduguda deposit (Fig. 4). The paragenetically oldest, Tourmaline-1, is represented by a) dark brown/yellow tourmaline in quartz-tourmaline rock and in meta-conglomerate, b) brown, irregular cores/relics in complexly optically zoned tourmaline in quartz-sulphides vein and chlorite schist, and c) dark green/brown tourmaline in biotite schist. The presence of stretched and boudinadged clusters of tourmaline, the occurrence of pressure-shadows around tourmaline grains and the common cataclastic texture of the grains and their parallel alignment with foliation collectively imply that Tourmaline-1 is pre-kinematic with respect to ductile shearing. The second stage of tourmaline growth, Tourmaline-2, is represented by light greenish blue/blue tourmaline occurring as overgrowths on, and fracture-filling in pre-existing grains of Tourmaline-1. The mode of occurrence and restricted presence of Tourmaline-2 in the strongly crushed U-Cu zone ("granular rock") indicate that the second stage growth likely took place during deformation. Finally, the third and youngest tourmaline stage, Tourmaline-3, is represented by radiating, large grains that overprints all earlier fabric and is thus post-kinematic.

4 Analytical Methods

4.1 Electron microprobe analysis

Tourmaline compositions were determined on polished and carbon-coated 2.5 cm round thin sections by wavelength-dispersive electron microprobe analyses at the GFZ in Potsdam. The CAMECA SX-100 microprobe was operated at 15 kV accelerating voltage and 20nA beam current. Natural oxide and silicate mineral reference materials were used for calibration and data reduction employed the method of Pouchou and Pichoir (1984). Our procedure for microprobe analysis was to routinely analyze two or more points from the core and rim portions of optically zoned grains to check for chemical variations. Tourmaline structural formulae were calculated by normalizing to 15 cations in the tetrahedral and octahedral sites (T + Z + Y) according to the suggestion of Henry and Dutrow (1996). The structural formulae are approximate to the extent that our chemical analyses are not complete; we did not determine B, H_2O, ferrous/ferric iron ratio, and minor elements such as Li and Zn, which may be present at sub-wt.% level.

4.2 Boron isotope determination

The boron isotope composition of tourmaline was determined by secondary ion mass spectrometry (SIMS) with the CAMECA ims6f instrument at the GFZ Potsdam. After electron microprobe analysis, the samples were re-polished with alumina and distilled water to remove the carbon coat, then ultrasonically cleaned with high purity ethanol and coated with a ~35 nm thick high purity gold coat.

The use of a liquid nitrogen cold trap provided a secondary ion source pressure in the lower 10^{-10} Torr range. For the boron isotopic analyses the ims6f employed a nominally 12.5 kV $^{16}O^-$ primary beam which was focused to about 10 µm diameter on the sample surface. The beam current was set at 8 nA or 4 nA, the lower current being required to maintain count rates for ^{11}B below 500 kHz. Prior to each analysis, a 3 minute preburn was used in order to remove the gold coat and to establish equilibrium sputtering conditions. The mass spectrometer was operated at mass resolving power $M/\Delta M \approx 1200$, sufficient to separate the isobaric interference of $^{10}B^1H$ on the ^{11}B mass station and the $^{9}Be^1H$ peak on ^{10}B. A 50 µm diameter contrast aperture, an 1800 µm field aperture (equivalent to a 150 µm field of view) and 50 V energy window were used without voltage offset. Each analysis consisted of 100 scans of the sequence $^{9.95}$background (0.1 seconds per cycle), ^{10}B (2 s) and ^{11}B (1 s) resulting in a total analysis time of about 10 minutes. Instrumental mass fractionation (IMF) and analytical quality were assessed by replicate analyses of tourmaline reference materials dravite (HS #108796), elbaite (HS #98144) and schorl (HS #112566) from the Harvard Mineralogical Museum (Dyar et al., 2001), and tourmaline B4 from Tonarini et al., (2003). We have carried out analysis in two different sessions (16th to 18th November, 2009 and 25th to 27th November, 2009). During both the analytical sessions the 1 sd individual uncertainties were typically below ±0.5‰ (Table 1) and the repeatability on reference samples averaged 1.3 and 0.6 ‰ (1 sd) for first session and second session respectively. The variation in observed mass fractionation among the different reference samples was 1.8 and 1.5 ‰ (1 s.d.) for the first and second session respectively, which we believe to be the best estimate for the trueness of the data set. Boron isotope compositions are reported in $\delta^{11}B$ notation ($\delta^{11}B = \{^{11}B/^{10}B_{sample}^{corr} / ^{11}B/^{10}B_{RM} - 1\} \times 1000$) relative to NBS SRM 951, whose $^{11}B/^{10}B$ ratio is taken as 4.04362 (Cantanzaro et al., 1970).

5 Chemical composition of tourmaline

All analyzed tourmalines classify in the alkali group of Hawthorne and Henry (1999) based on the A-site occupancy (Fig. 5a). Tourmalines are dravitic; in all but a few cases they plot on the Mg-rich side of the schorl-dravite join on the Al-Mg-Fe diagram (Fig. 5b) of Henry and Guidotti (1985). However, there is considerable deviation in Al from ideal schorl-dravite, with a large number of compositions being Al-deficient (< 6 apfu) and some Al-rich (also see Fig. 6e). Overall, the Fe/(Fe+Mg) and Na/(Na+Ca) values range from 0.17 to 0.53 and 0.69 to 0.93 respectively (Fig. 6a). The concentration of vacancies at the X-site ranges from near-zero to 0.15 pfu in most samples, with a maximum of 0.26 pfu(Fig. 6f).

Tourmaline from different rock types shows overlapping concentrations of Na, Ca and Al, but there are distinctive patterns in Fe, Mg and Ti concentrations that correlate with host lithology (Fig 6a to 6e). For example, on the Al-Mg-Fe plot (Fig. 5b) tourmaline from biotite schist (filled squares)

plots apart from other samples and defines a distinct trend towards the Al-free endmember povondraite ($(Na(Fe_3)(Fe_4Mg_2)(Si_6O_{18})(BO_3)(OH)_3(O))$). Other relationships are distinctive on the variation diagrams (Fig. 6). Tourmaline from hanging wall meta-conglomerate (circles) and ore zone biotite schist (filled squares) define separate groups, those in meta-conglomerate being richer in Mg and Ti, and poorer in Fe. The compositions of most tourmaline from the quartz-tourmaline rock (open triangles) plots with the field of meta-conglomerate. Tourmaline from quartz-sulphide vein and chlorite schist display strong compositional variation. The majority of data cluster in the groups defined by meta-conglomerate (plus quartz-tourmaline rock) and biotite schist with some straddling between clusters (Fig 6a, c, d, e). As discussed later, this compositional variation of tourmaline in chlorite schist and quartz-sulphide vein is the manifestation of large compositional variation between Tourmaline-1 and Tourmaline-2 in these rocks. Amongst the minor elements, F concentration (not shown; see Table 2) is slightly higher in meta-conglomerate compared to those in biotite schist. Chromium concentrations are generally below 0.5 % in most tourmaline excepting a few high concentrations in meta-conglomerate, quartz-tourmaline rock and in biotite schist (Table 2).

Some compositional variations in Jadugada tourmaline are significant in terms of element substitutions in that mineral. For instance, the trend of Al-deficient tourmaline towards povondraite mentioned above suggests a substitution of Al by Fe^{+3} , and this is further substantiated by a strong negative correlation between Fe (apfu) and Al (apfu) of tourmaline (Fig 6e). Interesting is that the data from different host rocks plot along separate and parallel arrays in Fig 6e. This suggests a common substitution mechanism but different starting compositions related to the contrast in host rock compositions. The relationship between Fe and Mg in tourmaline is complex (Fig. 6g). There is a weak to moderate negative correlation between the two elements in most individual rock types but and none at all in tourmaline from biotite schist (filled squares, Fig. 6g). This lack of correlation is attributed to the importance of Fe^{+3} that substitutes for Al and not Mg. Examination of the element variations relative to ideal exchange vectors in Figures 6e to 6g indicates complex and probably multiple substitution mechanisms are involved e.g. $(Fe^{+2}, Fe^{+3})(Mg^{+2}, Al^{+3})_{-1}$, $(Na, Fe^{+2})(\square, Al)_{-1}$, $FeMg^{+2}_{-1}$.

An important observation is that there are regular differences in composition among the three paragentic types of tourmalin, and this adds to the complexities of data trends shown in the variation diagrams of Fig. 6. For example, Tourmaline-2 in the quartz-sulphide vein and in chlorite schist, which forms greenish blue rims and fracture-fillings on and in patchy brown relict grains of Tourmaline-1, is significantly poorer in Ti and Mg, and richer in Fe and Al (Fig. 7a to 7d) compared to the early tourmaline in the same samples. The variation in Ca content between the two tourmaline generations is rather erratic in these two rocks. In contrast to this, Tourmaline-2 in biotite schist is consistently richer in Al and Ca than Tourmaline-1 in that rock type, and poorer in Fe. Here, the Mg variations between the two tourmaline generations are erratic and Ti remains nearly unchanged. These

contrasts in compositional differences between Tourmaline 1 and 2 in the different host rocks make sense when plotted together (Fig. 7). Whereas the variation in Tourmaline-1 compositions is strong and dependent on host lithology, it appears that Tourmaline-2 compositions converge (arrows on Fig. 7), and this convergence probably reflects the influence of hydrothermal fluid as discussed more in section 7.1.

6 Boron isotope composition of tourmaline

The tourmaline from the Jaduguda deposit covers a range of $\delta^{11}B$ values from -6.8 to +17.2 ‰ (Table 2, Fig. 8). Notwithstanding the wide range, most tourmaline has isotopically heavy values. The mean value of the entire data set (n = 66) is +5.7 ‰ with a standard deviation of 3.7 ‰. The important features of the B- isotopic composition of Jaduguda tourmaline, based on our results, are as follows:

1. The $\delta^{11}B$ values of tourmaline in footwall quartz-tourmaline rocks are all positive (Fig. 8a), between +4.5 and +9.1 ‰, with a mean value of +6.6 ‰ and standard deviation of 1.6 ‰ (n=13). The tourmaline from the hanging wall conglomerate (Fig. 8c) yields essentially the same $\delta^{11}B$ values as the footwall, from +4.3 to +9.6 ‰ with a mean of +6.6 ‰ and standard deviation of 1.4 ‰ (n= 12), . Within-sample isotopic variations in these rocks are less than 4 ‰ (compare with total analytical uncertainty of about 2 ‰), and no significant isotopic variation was found between grain cores and rim, in keeping with the textural, optical and compositional homogeneity of tourmaline in these rocks.Undoubtedly part of the reason for the relative isotopic and chemical homogeneity in these samples compared with the other group (below) is that only one generation of tourmaline is present (Tourmaline-1).

2. With few exceptions, the tourmaline from all host-rock types within the U-Cu ore zone is isotopically heavy (Fig. 8b), with 37 of 41 analyses yielding $\delta^{11}B$ values greater than zero. Spefically, the samples from biotite schist, quartz-sulphide vein and chlorite schist cover ranges of -6.8 to +17.2 ‰, -5.8 to +7.1 ‰, and +1.5 to +10.9 ‰, respectively. Thus there is major overlap in B-isotope composition of ore-zone tourmaline and tourmaline from the footwall and the hanging wall rocks, but the important differences are that the ore-zone tourmaline has a much broader range overall, and that within-sample variations are larger and in some cases extreme (up to +10 ‰) .

3. Much of the internal variation in tourmaline from the U-Cu zones is related to the presence of three stages of tourmaline growth in those rocks. The pre-kinematic Tourmaline-1 in the U-Cu zones has exclusively positive values, with the mean isotopic composition of +5.7 ‰. This is very similar to the +6.6 ‰ mean composition of Tourmaline-1 from the footwall and the hanging wall samples. In contrast, the $\delta^{11}B$ values of Tourmaline-2 grains from the ore-zone

samples range between -6.8 to +4.0 ‰. The overall ranges for the Tourmaline-1 and Tourmaline-2 overlap but where both generations are found in a single grain, Tourmaline-1 invariably has heavier isotopic compositions than Tourmaline-2 (Fig. 7d). Finally, the post-kinematic, radial grains of Tourmaline-3, found in biotite schist of the ore zone (Fig. 4g) has the same range of $\delta^{11}B$ values (+4 to +11.1 ‰) as Tourmaline-1 from the sample.

7 Discussion

7.1 Implications of compositional variation of tourmaline

It is well established that the major element composition of tourmaline is strongly influenced by the host rock composition and the Jadugada tourmalines are no exception. The clearest example of host-rock control is the compositional contrast between tourmaline from meta-conglomerate and quartz-tourmaline rock in the hanging wall and footwall zones on the one hand, and tourmaline from the biotite schist on the other (Fig. 6). The high modal proportion of biotite in the schist, and partitioning of F and Ti to biotite relative to tourmalinecan explain the lower concentration of these two elements in tourmaline from biotite schist compared to that in meta-conglomerate. High Cr contents in schist-hosted tourmaline likely reflects the original mafic protolith, whereas the high Cr and Ti content of tourmaline in meta-conglomerate presumably were derived from the release of Cr from original, detrital chromite/ferritchromite and Ti from Fe-Ti oxides. The aluminium-deficiency in tourmaline from most rocks and the good correlation of Al with Fe suggests a substitution of Al^{3+} by Fe^{3+} and this in turn implies oxidizing conditions during tourmaline growth in the samples. The presence of tiny haematite grains in the quartz-tourmaline rock, oxidized rims of ferritchromite on relict detrital chromite grains in meta-conglomerate, and the ubiquitous presence of uraninite in the analyzed samples support this proposition.

The contrasting compositions of Tourmaline-1 and Tourmaline-2 in individual rock types in the U-Cu zone suggest an additional control on tourmaline composition by the hydrothermal fluid. This is supported by the observation that Tourmaline-2 (rims or fracture-fillings) from the diverse rock types in the ore zone (i.e., quartz-sulphide vein, biotite schist, chlorite schist) show much less variation than Tourmaline-1 from the same samples. In other words, the later growth of tourmaline tends to converge toward a common composition (Fig. 7). The simplest explanation for this is that Tourmaline-2 compositions in all samples were influenced by hydrothermal fluid under a high water/rock ratio during deformation. The strong brecciation and cataclasis of the rocks and minerals in the U-Cu zone and ubiquitous chloritization of biotite indicates a combination of intense deformation and fluid flux (hydrothermal/metamorphic fluid) in this zone. Lower Ti-contents of Tourmaline-2 compared to Tourmaline-1 in the quartz-vein and chlorite schist suggest that the corresponding fluid was poor in Ti. However, almost identical Ti concentration in the two generations of tourmaline in

biotite schist supports the inference made above that Ti was buffered by the abundant presence of biotite. Higher Al contents (locally with excess Al) of Tourmaline-2 (Fig. 7a) may imply less-oxidizing fluid compared to that responsible for the formation of Tourmaline-1. The youngest, post-kinematic stage of tourmaline growth (radial Tourmaline-3) has a stronger compositional (and isotopic) similarity with Tourmaline-1 than with Tourmaline 2 in the same rock, suggesting that the late tourmaline formed by local recrystallization of Tourmaline-1.

7.2 Isotopic heterogeneity implies multiple fluid sources

The first-order feature of tourmaline from the U-Cu ore zone is the wide range in isotopic compositions and the heterogeneity at the scale of individual samples, locally even within single grains (Fig. 8). In principle, isotopic variations in tourmaline can result during growth from a single fluid if there is variable isotopic fractionation taking place between mineral and fluid during growth (Palmer and Slack, 1989). Alternatively, and more commonly, isotopic heterogeneity at the sample and mineral scale reflects the involvement of isotopically distinct multiple fluids focused into the site of tourmaline growth during a single or multiple events (e.g., Krienitz et al., 2008; Xavier et al., 2008; Jiang et al., 2008). Isotopic variation may also result from variable water/rock ratios if B is present in similar concentrations in both the fluid and the rocks it interacts with (Jiang et al., 1999). However, the very high modal percentage of tourmaline (up to about 50 vol%) in the Jaduguda samples we have studied implies that the high boron concentration must be externally derived and the isotopic composition of tourmaline will thus be dominated by that of the hydrothermal fluid. Experimental studies on tourmaline-water isotopic fractionation demonstrate that tourmaline preferentially takes up ^{10}B compared to the co-existing fluid and the difference in $\delta^{11}B$ between coexisting tourmaline and fluid is temperature dependent (Meyer et al., 2008). Based on the homogenization temperature of fluid inclusions (Mishra and Singh, 2003), the temperature for ore mineralization at Jaduguda can be considered as ~ 300 to 450°C. These values are not corrected for pressure and therefore represent minimum temperatures of fluid entrapment. According to the experimental results of Meyer et al., (2008), later confirmed by Marschall et al. (2009), the B- isotopic fractionation between tourmaline and fluid at 300 and 450°C is 3.8 ‰ and 2.3 ‰, respectively, and the effect diminishes at higher temperature. . Temperature variations during tourmaline growth may therefore contribute to the observed isotopic heterogeneity but the effect is much too small to explain the observed isotopic variations in the U-Cu ore zone. Rayleigh fractionation can produce much larger variations in isotopic composition than equilbrium fractionation alone. Evidence for Rayleigh fractionation of boron isotopes has been found in some tourmaline studies (e.g., Jiang et al., 1999; Trumbull et al., 2008). We show model curves for Rayleigh fractionation at 400°C with an initial fluid composition of +10 ‰ based on a mean value of Tourmaline-1 grains from foot- and hanging wall samples, and a fluid fractionation factor of about 3 ‰. The model predicts progressively heavier isotopic compositions of later generation tourmaline (Fig. 8e), which is contrary to the observed differences between

Tourmaline-1 and 2 (Fig. 8d). Therefore, we propose that the consistently positive $\delta^{11}B$ values of early Tourmaline-1 on the one hand (represented by all tourmaline in quartz-tourmaline rock and meta-conglomerate, and by Tourmaline-1 in U-Cu zone rocks), and the isotopically lighter, commonly negative $\delta^{11}B$ values of Tourmaline-2 on the other hand (restricted to the ore zone), represent two isotopically distinct fluids. We attribute the compositional and isotopic similarity of post-deformation Tourmaline-3 and Tourmaline-1 to recrystallization of the earlier tourmaline to form the later. A late influx of fluid(s) compositionally similar to those involved in growth of Tourmaline-1 is also possible.

Tourmaline-1 is characterized by exclusively heavy B-isotopic compositions but there is still a significant spread in $\delta^{11}B$ values for the first-stage tourmalines in the different samples which needs explanation (from ~ +5‰ in the U-bearing footwall and hanging wall rocks to as high as ~ +15 ‰ in the U-Cu zone rocks). As described above, simple temperature variations and fluid-mineral fractionation cannot produce isotopic contrasts of this magnitude . Metamorphic recrystallization of tourmaline and interaction with metamorphic fluid can cause isotopic heterogeneity (Slack et al., 1993; Pesquera et al., 2005), and we are uncertain whether the cumulative effect of initial heterogeneity (hydrothermal stage) and a metamorphic overprint in the Singhbhum shear zone can explain the isotopic variation in Jaduguda Tourmaline-1. In their study of primary fluid inclusions from the Jaduguda deposit, Mishra and Singh (2003) demonstrated the presence of two compositionally distinct fluids in the mineralized zone, a high salinity brine and a low salinity presumably meteoric water. It is possible therefore that the range in the isotopic composition of Tourmaline-1 resulted from mixing of two fluids with different isotopic signatures. The possible origin of these fluids is discussed in section 7.3.

7.3 Sources of hydrothermal fluid

It is apparent from the above discussion that isotopically heavy fluid(s) participated in the precipitation of Tourmaline-1 both in the U-Cu ore zone and its footwall and hanging wall side. Isotopically lighter fluid was focussed into the U-Cu zone at a later stage, presumably during deformation. Considering the lower-end temperature of ore formation as 350°C (Mishra and Singh, 2003), the $\delta^{11}B$ value of the hydrothermal fluid responsible for the formation of Tourmaline-1was in the range of ~+6‰ to ~+20 ‰ using the fluid-tourmaline fractionation data of Meyer et al. (2009). Continental boron sources (sediments, granites, nonmarine evaporites) have moderate to strongly negative $\delta^{11}B$ values (Chaussidon and Albarede, 1992; Palmer and Swihart 1996; Kaseman et al., 2000; Marschall and Ludwig, 2006) and therefore cannot be important in the case of Jaduguda. TMore likely boron sources for the high$\delta^{11}B$ values of pre-deformation tourmaline from Jaduguda deposit are rocks with a marine affinity: seafloor-altered oceanic crust, marine sediments or evaporites, or arc volcanic rocks affected by subduction-zone fluids. Of the potential source rocks for isotopically heavy boron, altered oceanic

crust, marine sediments and arc volcanics have variable and overlapping $\delta^{11}B$ values that rarely exceed +10‰ (Palmer and Swihart, 1996; Jiang et al., 1999, Peacock and Hervig 1999; Nakano and Nakamura 2001). Given the range of possible $\delta^{11}B$ values (+6 to +20 ‰) we cannot uniquely distinguish the source of boron for Tourmaline-1 at Jaduguda, but the upper end of this range near 20 ‰ can best be ascribed to marine evaporites, carbonate or entrained sea water (Palmer and Slack, 1989; Palmer and Swihart, 1996; Jiang et al., 1997). There are several other pieces of evidence for modified sea-water, e.g. evaporite or basinal brine as the source of contained boron in Tourmaline-1 in the Jaduguda deposit. One is the high modal concentration of tourmaline itself, which implies a fluid much more enriched in boron than entrained seawater. Also, as mentioned above, the primary fluid inclusions in quartz from Jaduguda (Mishra and Singh, 2003) demonstrate the ubiquitous presence of high salinity (~ 50 wt% NaCl equivalent) brine in the ore zone. High salinity (~50% NaCl equivalent) fluid inclusions with barite daughter crystals were found in tourmaline from tourmaline-rich feldspathic schist in the Singhbhum shear zone outside the Jaduguda deposit (Pal et al., 2008). Other indications for high salinity fluid in alteration and mineralization are the presence of Cl-rich biotite, amphibole and locally scapolite (up to 3 wt.% Cl) in and around the Jaduguda deposit (Das, 2009; Unpublished data of DCP), and the extensive alkali alteration in the shear zone. Finally, a study of sulphur isotope variations in pyrite from the Jaduguda deposit (Sarkar, 2009; unpublished data of DCP) found mostly values, which implies reduction of probable seawater sulphate.

It must be said that no meta-evaporite has yet been recognized in the Singhbhum shear zone. It is possible that due to low preservation potential during metamorphism and deformation, evaporitic rocks are no longer preserved or no longer recognized as such.

The paragenetically late Tourmaline-2 has a consistently lighter isotopic compositions compared to Tourmaline-1 and it was argued above that this requires a different boron source. Since the progressive deformation in the Singhbhum shear zone was associated with prograde metamorphism, this tourmaline can be considered as syn-metamorphic. For a peak metamorphic temperature of 480 ± 40°C for the shear zone rocks (Sengupta et al., 2005) the isotopic composition of fluid in equilibrium with Tourmaline-2 had a range of of - 4.8 to +6.0 ‰ using the fractionation data from Meyer et al., (2008). This is in good agreement with the range of $\delta^{11}B$ values for a number of common volcanic and metamorphic rock (e.g. Barth 1993; Chaussidon and Jambon, 1994; Palmer and Swihert, 1996). Hence the simplest explanation for this isotopic signature of Tourmaline-2 is derivation of boron from the metamorphic volcano-sedimentary sequences in and around the shear zone.

7.4 Implications for a metallogenetic model

It is recalled that diverse ore genetic models have been proposed for polymetallic mineralization in the Singhbhum shear zone , including magmatic-hydrothermal, metamorphogenic, volcanogenic-exhalative massive sulphides (VMS) and iron oxide-copper-gold (IOCG). The lack of associated granitic intrusions of appropriate age and the widespread evidence for high-salinity fluid in pre-deformation mineralization and alteration rules out the magmatic-hydrothermal model. Strongly positive boron isotopic signatures like those of Tourmaline-1 from Jaduguda have been recently reported from tourmaline in IOCG-style deposits from Brazil and the USA (Xavier et al., 2008, Trumbull et al., in press), and the involvement of marine evaporite-derived fluid in IOCG deposits has been invoked (see also Barton and Johnson, 1996; 2000). According to the review of Palmer and Slack (1989), theδ^{11}B values of tourmaline from volcanogenic massive sulphide deposits (VMS) are mostly negative to weakly positive, but there are examples of VMS deposits with marine evaporites or carbonates in the sequence that contain tourmaline with heavy boron isotope compositions Of course, the boron isotope compositions of tourmaline alone cannot distinguish whether the Jaduguda deposit belongs to the VMS or IOCG association, but the high δ^{11}B values add support to a number of other features of the Jaduguda deposit which are most consistent with a variant of IOCG-type mineralization (*cf* Hitzman et al., 1992; Williams et al., 2005). These include the characteristic metal association, notably including Fe, Cu and U, and the lack of Zn sulphide mineralization that is typical for VMS deposits. Magnetite is abundant in the mineralized shear zone and is produced as a byproduct in Jaduguda. In addition to the magnetite association with sulphides and uraninite, there are also many occurrences of magnetite-apatite mineralizations that are known to be REE-bearing (e.g., apatite with up to ~0.4% REE; Sarkar, 1984). Several REE-bearing minerals (Sarkar, 1982; 1984; Unpublished data of DCP) and trace element rich pyrite (particularly Co and Ni) are ubiquitous in the mineralized shear zone and specifically in the Jaduguda deposit (Pal et al., 2009; Sarkar, 2009; Chowdhury and Pal, 2009). IOCG-like alkali and acid alteration is widespread, as exemplified by extensive albite-dominated feldspathic schist, biotite schist and chlorite schist. All these features along with ubiquitous presence of high salinity fluid in the mineralized zone are consistent with an IOCG-type mineralization in Jaduguda and we believe that this is also the best explanation for the heavy B-isotope compositions of tourmaline from the deposit reported here.

8 Conclusions

1. The host rocks of U ± base metal mineralization in the Jaduguda polymetallic deposit are characteristically rich in alkali tourmaline of dravite-schorl compositions. Three generations of tourmaline are recognized. Pre-kinematic Tourmaline-1 is ubiquitous in the U-Cu ore zone, comprising biotite schist, chlorite schist and quartz-sulphide veins, and is also found in the footwall quartz-tourmaline rock and hanging wall meta-conglomerate. Syn-kinematic Tourmaline-2 and post-kinematic Tourmaline-3 occur only in the U-Cu ore zone. Compositional contrast of pre-kinematic

tourmaline in different rock types suggests a firsthand control of host rock on tourmaline composition. The hydrothermal fluid responsible for the formation of first generation pre-kinematic tourmaline was oxidizing as indicated by the inferred presence of Fe^{3+} and compositional trend towards povondraite. The compositional convergence of syn-deformation tourmaline in different rock types in the brecciated U-Cu zone indicates a control of hydrothermal fluid on the compositions of this tourmaline under high water/rock ratio. Compositional similarity of post-kinematic tourmaline with the pre-kinematic tourmaline in the same rock indicates redistribution of existing materials or formation of this tourmaline by a process similar to that which formed pre-kinematic tourmaline.

2. Boron isotope compositions of different tourmaline generations in the U-Cu zone indicate influx of isotopically distinct fluid in the site of tourmaline growth over a protracted period of time during the evolution of the Singhbhum shear zone. The earliest recognizable event of hydrothermal mineralization was associated with influx of marine evaporite-derived fluid producing pre-kinematic and pre-metamorphism U (footwall and hanging wall) and U + Cu (main polymetallic ore zone) concentration. Subsequently, during deformation and metamorphism either a metamorphic fluid or an externally derived fluid that equilibrated with the surrounding metamorphic volcano-sedimentary country rocks was focused into the zone of brecciation and cataclasis. Occurrence of this tourmaline generation and chalcopyrite both in association with chloritization likely suggests additional base metal mineralization (or mobilization and concentration of existing sulphide) facilitated by syn-kinemaic and syn-metamorphic fluid flux. A less pervasive post-deformation and post-metamorphism fluid event may have resulted in minor addition/mobilization of Cu in the ore zone as evident from minor chalcopyrite associated with post-deformation tourmaline. Isotopic (and compositional) similarity of this tourmaline with that of pre-kinematic tourmaline indicates that the latter grew either through local recrystallization or by a process similar to the one that formed pre-kinematic tourmaline.

3. The heavy B- isotopic compositions of pre-kinematic tourmaline support other geological and geochemical evidence for an Fe oxide (Cu-U-REE) (IOCG)- style mineralization in the Jaduguda U (-Cu-Fe) deposit. However, more detailed study involving alteration types and alteration patterns vis-a-vis ore mineralization is warranted for a comprehensive metallogenetic model.

Acknowledgements

The present work was initiated with a financial grant from DST, Govt. Of India in the form of Fast Track Young Scientist project to DCP (SR/FTP/ES-24/2004). The compositional and isotopic characterization of tourmaline was carried out in the GFZ, Potsdam, Germany during a three months' visit of DCP under INSA-DFG bilateral exchange program. The Chairman and Managing Director, Uranium Corporation of India Limited (UCIL) is thanked for his permission to work in and collect samples from the Jaduguda mine. Shri A.K. Sarangi, Shri S Das, and Shri A.S. Singh of UCIL were of

immense help during the field work. Oona Appelt of electron microprobe laboratory and Ilona Schäpan of SIMS laboratory in GFZ, Potsdam are thanked for their help during the analysis. Marc-Sebastian Krienitz is thanked for fruitful discussions on tourmaline compositions and for his help during the course of the study. We extend our sincere thanks to the editor, Bernard Bourdon and reviewers Horst Marschall and Shao-Yong Jiang for critically reviewing the article and for their suggestion that helped us to improve the manuscript.

References

Aug´e, T., Cocherie, A., Genna, A., Armstrong, R., Guerrot, C., Mukherjee, M.M., Patra, R.N., 2003. Age of the Baula PGE mineralization (Orissa, India) and its implications concerning the Singhbhum Archaean Nucleus. Precambrian Research 121, 85–101

Banerjee, P.K., 1982. Stratigraphy, petrology and geochemistry of some Precambrian basic volcanic and associated rocks of Singhbhum District, Bihar and Mayurbhanj and Keonjhar districts, Orissa. Geological Survey of India Memoir 111, 54 pp

Banerji, A.K., 1962. Cross-folding, migmatization and ore localisation along parts of the Singhbhum shear zone, south of Tatanagar, Bihar, India. Economic Geology 57, 50–71

Banerji, A.K., 1981. Ore genesis and its relationship to volcanism, tectonism, granitic activity and metasomatism along the Singhbhum shear zone, Eastern India. Economic Geology 76, 905–912

Banerji, A.K., Talapatra, A., 1966. Soda-granites from south of Tatanagar, Bihar, India. Geological Magazine 103, 340–351

Barth, S., 1993. Boron isotope variations in nature: a synthesis. Geologische Rundschan 82, 640–651

Barton, M.D., Johnson, D.A., 1996. Evaporitic source model for igneous-related Fe-oxide (REE–Cu–Au–U) mineralization. Geology 24, 259–262

Barton, M.D., Johnson, D.A., 2000. Alternative brine sources for Fe-oxide (–Cu–Au) systems: Implications for hydrothermal alteration and metals. In Porter, T. M., ed. (Ed.) Hydrothermal iron oxide copper-gold and related deposits: A global perspective. Adelaide, Australian Mineral Foundation. 2: 43–60

Bhattacharya, H.N., Chatterjee, A., Chowdhury, S., 1992. Tourmalinite from Cu-U Belt of Singhbhum, Bihar, India. Journal of the Geological Society of India 39, 191−195.

Cantanzaro, E.J., Champion, C.E., Garnet, E.L., Maienko, G., Sappenfield, K.M., Shields, W.R., 1970. Boric acid:isotopic and assay standard reference materials. National Bureau Standards (US). Special Publication 260-17, 70p

Changkakoti, A., Gray, A., Morton, R. D., Sarkar, S. N., 1987. The Mosabani Copper Deposit, India – A preliminary study on the Nature and genesis of ore fluids. Economic Geology 82, 1619–1625.

Chaussidon, M., Jambon, A., 1994. Boron content and isotopic composition of oceanic basalts: geochemical and cosmochemical implications. Earth and Planetary Science Letters. 121, 277–291

Chowdhury, S., Pal, D. C., 2009. Trace element compositions of pyrite in Surda Cu deposit-implications in chemical evolution of mineralization. IAGR Conference Series No. 9, IGCP-509. Indian Statistical Institute, India. 23-24

Das, H., 2009. Hydrothermal alteration and ore mineralization in the Jaduguda uranium deposit, Singhbhum shear zone, eastern India. Unpublished MSc. Thesis, Jadavpur University, Kolkata, India. pp 40

Dunn, J.A., Dey, A.K., 1942. Geology and Petrology of Eastern Singhbhum and surrounding areas. Geological Survey of India Memoir 69 (2).

Dyar, M.D., Wiedenbeck, M., Robertson, D., Cross, L.R., Delaney, J.S., Ferguson, K., 2001. Reference minerals for microanalysis of light elements. Geostandards Newsletter 25, 441–463

Ghosh, A. K., 1972. Trace element geochemistry and genesis of the copper ore deposits of the Singhbhum shear zone, Eastern India: Mineralium Deposita 7, 292–313.

Ghosh, S.K., Sengupta, S., 1987. Progressive development of structures in a ductile shear zone. Journal of Structural Geology 9, 277−287

Ghosh, S.K., Sengupta, S., 1990. Singhbhum shear zone: structural transition and kinematic model. Proceedings of the Indian Academy of Science (Earth Planetary Science) 99, 229−247

Gupta, A., Basu, A., Singh, S.K., 1985. Stratigraphy and petrochemistry of Dhanjori Greenstone belt, Eastern India. Quaterly Journal of the Geological Mining and Metallurgical Society of India 57, 248– 63.

Hawthorne, F.C., Henry, D.J., 1999. Classification of the minerals of the tourmaline group. European Journal of Mineralogy 11, 201–215

Henry, D.J., Dutrow, B.L., 1996. Metamorphic tourmaline and its petrologic applications. In: Grew, E.S., Anovitz, L.M., (Eds.), Boron: Mineralogy, Petrology and Geochemistry. Reviews in mineralogy 33, 503–558

Henry, D.J., Guidotti, C.V. 1985. Tourmaline as a petrogenetic indicator mineral: an example from the staurolite-grade metapellites of NW Maine. American Mineralogist 70, 1–5

Hitzman, M.W., Oreskes, N., Einaudi, M.T. 1992. Geological characteristics and tectonic setting of Proterozoic iron oxide (Cu–U–Au–REE) deposits. Precambrian Research 58, 241–287

Jiang, S.-Y., Palmer, M.R., Peng, Q.-M., Yang, J.-H., 1997. Chemical and stable isotopic compositions of Proterozoic metamorphosed evaporites and associated tourmalines from the Houxianyu borate deposit, eastern Liaoning, China. Chemical Geology 135, 189-211

Jiang, S.-Y., Palmer, M.R., Slack, J.F., Shaw, D.R., 1999. Boron isoope systematic of tourmaline formation in the Sullivan Pb-Zn-Ag deposit, British Columbia, Canada. Chemical Geology 158, 131–144

Jiang, S.-Y., Radvanec, M., Nakamura, E., Palmer, M., Kobayashi, K., Zhao, H.-X., Zhao, K.-D., 2008. Chemical and boron isotopic variations of tourmaline in the Hnilec granite-related hydrothermal system, Slovakia: Constraints on magmatic and metamorphic evolution. Lithos 106, 1-11

Kasemann, S., Erzinger, J., Franz, G., 2000. Boron recycling in the continental crust of the central Andes from the Paleozoic to Mesozoic, NW Argentina. Contributions to Mineralogy and Petrology 140, 328–343

Krienitz, M.-S., Trumbull, R. B., Hellmann, A., Kolb, J., Meyer, F. M., Wiedenbeck, M., 2008. Hydrothermal gold mineralization at the Hira Buddini Gold Mine, India: constraints on fluid sources and evolution from boron isotopic compositions of tourmaline. - Mineralium

Deposita 43, 4, 421-434

Marschall, H.R., Ludwig, T., 2006. Re-examination of the boron isotopic composition of tourmaline from the Lavicky granite, Czeck Republic, by secondary ion mass spectometry: back to normal. Geochemical Journal 40, 631-638

Marschall, H.R., Meyer, C., Wunder, B., Ludwig, T., Heinrich, W. 2009. Experimental boron isotope fractionation between tourmaline and fluid: confirmation from in situ analysis by secondary ion mass spectrometry and from Rayleigh fractionation modelling. Contributions to Mineralogy and Petrology 158, 675-681

Mazumder, R., Sarkar, S. 2004. Sedimentation history of the Palaeoproterozoic Dhanjori Formation, Singhbhum, eastern India. Precambrian Research 130, 267–287

Mazumder, R., 2005. Proterozoic sedimentation and volcanism in the Singhbhum crustal province, India and their implication. Sedimentary Geology 176, 167–193

Meyer, C., Wunder, B., Meixner, A., Romer, R.L., Heinrich, W., 2008. Boron isotope fractionation between tourmaline and fluid: an experimental re-investigation. Contributions to Mineralogy and Petrology 156, 259–267

Misra, S., Johnson, P.T., 2005. Geochronological constrains on evolution of Singhhbum Mobile Belt and associated basic volcanics of eastern Indian shield, Gondwana Research 8, 129–142

Misra, S., Deomuarari, M.P., Wiedenbeck, M., Goswami, J.N., Ray, S., Saha, A.K., 1999. $^{207}Pb/^{206}Pb$ zircon ages and the evolution of the Singhbhum Craton, eastern India: an ion microprobe study. Precambrian Research 93, 139–151

Mishra, B., Pal, N., Ghosh, S., 2003. Fluid evolution of the Mosabani and Rakha copper deposits, Singhbhum district, Jharkhand: evidence from fluid inclusion study of mineralized quartz veins. Journal of the Geological Society of India 61, 51−60

Mishra, B., Singh, R.K., 2003. Fluid evolution of the Jaduguda U–Cu deposit, Jharkhand. Indian Journal of Geology 75, 191–202

Moorbath S, Taylor PN, Jones NW (1986) Dating the oldest terrestrial rocks- fact and fiction. Chemical Geology 57:63–86

Mukhopadhyay, J., Beukes, N.J., Armstrong, R.A., Zimmermann, U., Ghosh, G., Medda R.A., 2008. Dating the Oldest Greenstone in India: A 3.51-Ga Precise U-Pb SHRIMP Zircon Age for Dacitic Lava of the Southern Iron Ore Group, Singhbhum Craton. Journal of Geology. 116, 449–461

Nakano, T., Nakamura, E. 2001. Boron isotope geochemistry of metasedimentary rocks and tourmaline in a subduction zone metamorphic suite. Physics of Earth and Planet Interiors 127, 233–252

Pal, D.C., Barton, M.D., Sarangi, A.K. 2009. Deciphering a multistage history affecting U-Cu (-Fe) mineralization in the Singhbhum Shear Zone, eastern India using pyrite textures and compositions in the Turamdih U-Cu (-Fe) deposit. Mineralium Deposita 44, 61–80

Pal, D.C., Saravanan, S., Mishra, B., 2008. Involvement of high temperature oxidized brine in pre-shearing hydrothermal alteration: evidence from fluid inclusions in tourmaline in feldspathic schist, Pathargora area, Singhbhum shear zone, eastern India. Abstracts with program of the second meeting of the Asian Current Research on Fluid Inclusions (ACROFI-2). IIT, Kharagpur, India.

Palmer, M.R., Slack, J.F., 1989. Boron isotopic composition of tourmaline from massive sulphide deposits and tourmalinites. Contributions to Mineralogy and Petrology 103, 434–451

Palmer, M.R., Swihart, G.H., 1996. Boron isotope geochemistry: an overview. In: Grew, E.S., Anovitz, L.M., (Eds.), Boron: Mineralogy, Petrology and Geochemistry (Reviews in Mineralogy 33, 709–744

Pandey, P., Kumar, P., Upadhyay, L.D. ,1994. Uranium deposits of Turamdih-Nandup area, Singhbhum District, Bihar and their spatial relationship. Exploration and Research for Atomic Minerals 7, 1–13

Peacock, S.M., Hervig, R.L., 1999. Boron isotopic composition of subduction-zone metamorphic rocks. Chemical Geology 160, 281–290

Pesquera, A., Torres-Ruiz, J., Gil-Crespo, P.P., Jianga, S.-Y. 2005. Petrographic, chemical and B-isotope insights into the origin of tourmaline-rich rocks and boron recycling in the Martinamor antiform (central Iberian zone, Salamanca, Spain). Journal of Petrology 46, 1013–1044

Pouchou J.L., Pichoir, F., 1984. An new model of quantitative X-ray microanalysis-part I: application to the analysis of homogeneous samples. La Recherche Aerosp 3, 13–38

Rao, N.K., Rao, G.V.U., 1983. Uranium mineralization in Singhbhum Shear Zone, Bihar: IV: Origin and geological timeframe. Journal of the Geological Society of India 24, 615–627,

Roy, A., Sarkar, A., Jeyakumar, S., Aggrawal, S.K., Ebihara, M., 2002. Sm–Nd age and mantle source characteristics of the Dhanjori volcanic rocks, Eastern India. Geochemical Journal 36, 503–518.

Saha, A.K., 1994. Crustal evolution of Singhbhum North Orissa, Eastern India. Geological Society of India memoir 27, p. 341.

Saha, A.K., Ray, S.L, Sarkar, S.N. 1988. Early history of the Earth: evidence from the eastern Indian Shield. In: Mukhopadhyay, D. (Ed.), Precambrian of the Eastern Indian Shield. Geological Society of India Memoir 8, 13–37.

Sarkar, S., 2009. Trace element and sulfur isotope composition of pyrite in Jaduguda, Bhatin and Bagjata uranium mines, Singhbhum Shear zone, eastern India: implication in ore genesis. Unpublished MSc. Thesis, Jadavpur University, Kolkata, India. pp 37.

Sarkar, S.C., 1982. Uranium (-nickel-cobalt-molybdenum) mineralization along the Singhbhum copper belt, India, and the problem of ore genesis. Mineralium Deposita 17, 257-278

Sarkar, S.C., 1984. Geology and ore mineralisation along the Singhbhum copper uranium belt, Eastern India. Jadavpur University Press, Calcutta, p. 263

Sarkar, S.C., Deb, M., 1971. Dhanjori basalts and some related rocks. Quaterly Journal of Geological Mining and Metallurgical Society of India 43, 29–37

Sarkar, S.C., Deb, M., 1974. Metamorphism of the sulfides of the Singhbhum copper belt, India- the evidence from the ore fabric. Economic Geology 68, 1283–1293

Sengupta, N., Mukhopadhyay, D., Sengupta, P., Hoffbauer, R., 2005. Tourmaline-bearing rocks in the Singhbhum shear zone, eastern India: evidence of boron infiltration during regional metamorphism. American Mineralogist 90, 1241–1255

Sengupta, S., Ghosh, S.K., 1997. The kinematic history of the Singhbhum shear zone. Proceedings of the Indian Acadademy of Science (Earth planetary Science) 106, 185–196

Sharma, M., Basu, A.R., Ray, S.L., 1994. Sm-Nd isotopic and geochemical study of the Archaean tonalite–amphibolite association from the eastern India craton. Contributions to Mineralogy and Petrology 117, 45−55

Slack, J.F., Palmer, M.R., Stevens, B.P.J., Barnes, R.G., 1993. Origin and significance of tourmaline-rich rocks in the Broken Hill district, Australia. Economic Geology 88, 505–541

Srivastava, D.C., Pradhan, A., 1995. Late brittle tectonics in a Precambrian ductile belt: evidence from brittle structures in the Singhbhum Shear Zone, eastern India. Journal of Structural Geology 17, 385–396

Talapatra, A.K., 1968. Sulfide mineralization associated with migmatisation in the south-eastern part of the Singhbhum shear zone, Bihar, India. Economic Geology 63, 156–165

Tonarini, S., Pennisi, M., Adorni-Braccesi, A., Dini, A., Ferrara, G., Gonfiantini, R., 2003. Intercomparison of Boron isotope and concentration measurements. Part I: selection, preparation and homogeneity tests of the intercomparison materials. Geostandards Newsletter 27, 21–39

Trumbull, R. B., Krienitz, M.-S., Gottesmann, B., Wiedenbeck, M., 2008. Chemical and boron-isotope variations in tourmalines from an S-type granite and its source rocks: the Erongo granite and tourmalinites in the Damara Belt, Namibia. Mineralogy and Petrology, 155, 1, 1-18

Trumbull, R.B., Slack, J.F., Kreinitz, M-S., Belkin, H.E., Wiedenbeck, M., (in press). Fluid sources and metallogenesis in the Blackbird Co-Cu-Au-Bi-Y-REE district, Idaho, U.S.A.: constraints from chemical and boron isotopic variations in tourmaline. Canadian Mineralogist

Venkataraman, K., Shastry, S., Srinivasan, M. N., 1971. Certain observations regarding uranium and base metal mineralization. Proceedings of the Indian National Science Academy 37A, 131–144

Virnave, S.N., Mukhopadhaya, T.K, Krishnabadri, N.S.R., 1994. On some aspects of Stratigraphy, Depositional environment and its bearing on uranium mineralisation in parts of Singhbhum Shear Zone, Bihar. Jouranl of the Geological Society of India 43, 557– 571.

Williams, P., Barton, M.D., Johnson, D.A., Fontboté, L., Haller, A., Mark, G., Oliver, N.H.S., Marschik, R. 2005. Iron oxide copper-gold deposits: Geology, Space-time distribution, and possible modes of origin. Economic Geology 100th Anniversary volume, 371–405

Xavier, R.P., Wiedenbeck, M., Trumbull, R.B., Dreher, A.M., Monteiro, L.V.S., Rhede, D., de Araújo, C.E.G., Torresi, I. (2008): Tourmaline B-isotopes fingerprint marine evaporites as the source of high salinity ore fluids in iron oxide-copper-gold deposits, Carajás Mineral Province (Brazil). Geology 36, 743–746.

List of figures

Figure 1: Simplified geological map of the eastern Indian craton (Redrawn from Saha, 1994)

Figure 2: Lithological map around Jaduguda deposit (Redrawn from Deb and Sarkar, 1975)

Figure 3: Idealized section showing different rock types and two uranium lodes (footwall and hanging wall) along a cross-cut in th 555 m level in Jaduguda uranium mine. The vertical scale is exaggerated for easy recognition of different symbols.

Figure 4: Microphotographs of tourmaline from different rock types. All photographs except (e) are under plane polarized transmitted light. Figure (e) is taken under reflected light. a) Brown tourmaline from the footwall quartz-tourmaline rock. Note that the schistosity warps around tourmaline clusters; b) Fractured brown tourmaline in the hanging wall conglomerate; c) Complexly zoned tourmaline in the quartz-sulphide vein. Note that multiple irregular relicts of brownish yellow Tourmaline-1 (marked with dotted line) are surrounded and partly penetrated by light blue Tourmaline-2; d) Similar to figure (c) showing penetration (replacement/alteration?) of blue Tourmaline-2 in to Tourmaline-1. e) Inclusion riddled Tourmaline-1 core is rimmed by inclusion-free Tourmaline-2 rim in the biotite schist; f) Micro-cracks in brown Tourmaline-1 are filled with bluish Tourmaline-2 in biotite schist; g) Cluster of radiating Tourmaline-3 overprints foliation defined by biotite in the biotite schist; g) Bluish Tourmaline-2 rims and penetrates brown Tourmaline-1 in the chlorite schist. Numerals on the figures are $\delta^{11}B$ values. Note the strong heterogeneity in $\delta^{11}B$ values in a single grain of tourmaline.

Figure 5: a) Ternary classification of the Jaduguda tourmalines after Hawthorne & Henry (1999) based on the principal constituents at the X-site; b) Al-Fe-Mg ternary diagram after Henry and Guidotti (1985) with the compositions of Jaduguda tourmaline. Note that the tourmaline compositions trend across schorl-dravite join. Al-deficient tourmaline follows a trend towards the povondraite composition ($Na(Fe_3)(Fe_4Mg_2)(Si_6O_{18})(BO_3)(OH)_3(O)$). Labelled fields are: (1) Li-rich granitoid pegmatite and aplites, (2) Lithium-poor granitoids, pegmatites and aplites, (3) Fe^{3+}-rich quartz-tourmaline rocks (altered granitoids), (4) metapellites and metapsammites with Al-saturating phases, (5) metapellites and metapsammites lacking Al-saturating phases, (6) Fe^{3+}-rich quartz-tourmaline rocks, calc-silicate rocks and metapelites, (7) low-Ca metaultramafic rocks and Cr-V-rich metasediments, (8) meta-carbonates and meta-pyroxenites

Figure 6: Chemical compositions of tourmalines expressed in terms of atomic ratio and atoms per formula unit (a.p.f.u.). a) Fe/((Fe+Mg) versus Na/(Na+Ca), b) Ti a.p.f.u versus Fe a.p.f.u., c) Ti a.p.f.u. versus Mg a.p.f.u., d) Ti a.p.f.u versus Ca a.p.f.u., e) Total Al ap.f.u versus Fe a.p.f.u, f) Mg versus X-site vacancy and g) Fe versus Mg. Note that in all the plots, tourmaline from hanging wall conglomerate and those from biotite schist define two distinct clusters. Compositions of tourmaline from quartz-tourmaline rocks are mostly in the group defined by meta-conglomerate, whereas those from quartz-sulfide vein and chlorite schist are distributed in the two groups with some straddling the boundary. The exchange vectors are shown in figures e, f and g.

Figure 7: Examples of compositional zoning in tourmaline from the deformed, brecciated U-Cu zone encompassing biotite schist, chlorite schist and quartz-sulphide veins. The arrow heads point towards Tourmaline-2 that occurs as overgrowth or as fracture-filling on Tourmaline-1. Note compositional convergence of Tourmaline-2 in all the figures. Also note significant difference in Ti-concentration between Tourmaline-1 and Tourmaline-2 in quartz-sulphide vein and chlorite schist. Titanium concentrations in Tourmaline-1 and Tourmaline-2 are very similar in the biotite-schist.

Figure 8: Frequency histogram of boron isotope compositions of tourmaline from the footwall U-bearing quartz-tourmaline rock (a), U-Cu zone (b), and hanging wall U-bearing meta-conglomerate (c). Note the similarity in isotopic compositions of Tourmaline-1 in all zones and a distinctly lighter isotopic signature of Tourmaline-2 (rims/fracture-filling) in the Cu-U zone. Post deformation Tourmaline-3 displays similar isotopic compositions as that of Tourmaline-1. Arrows in (d) illustrate the extreme isotopic shift to lower values from Tourmaline-1 to Tourmaline-2 (at arrow heads) in some samples. Rayleigh fractionation curves in (e) demonstrate that the lower $\delta^{11}B$ values of Tourmaline-2 cannot be caused by fractionation effects alone, but must reflect a separate fluid component (see text).

Table captions

Table 1: Summary of SIMS boron isotopic analysis on reference materials

Table 2: Representative chemical and boron isotopic compositions of tourmaline from Jaduguda deposit

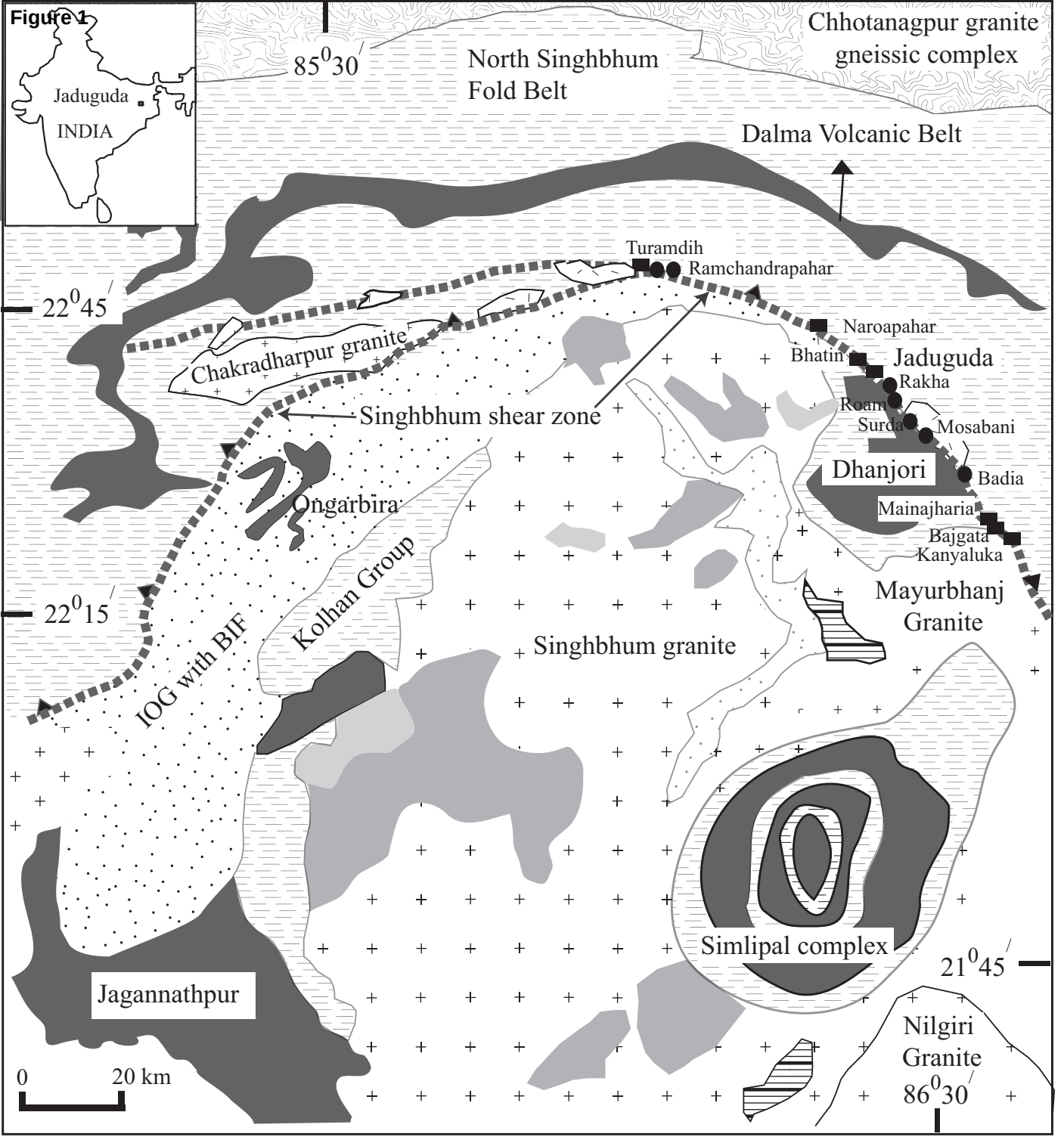

LEGEND

Older Metamorphic Group (Supra-crustals)

Older Metamorphic Tonalitic Gneiss (OMTG)

Iron Ore Group (IOG) greenstone sequence with BIF

Granitoids

Ultramafic intrusives

Volcanic sequence

Sedimentary sequence

Feldspathic schist

Singhbhum shear zone

Deposit locations

Uranium

Copper

Figure 2

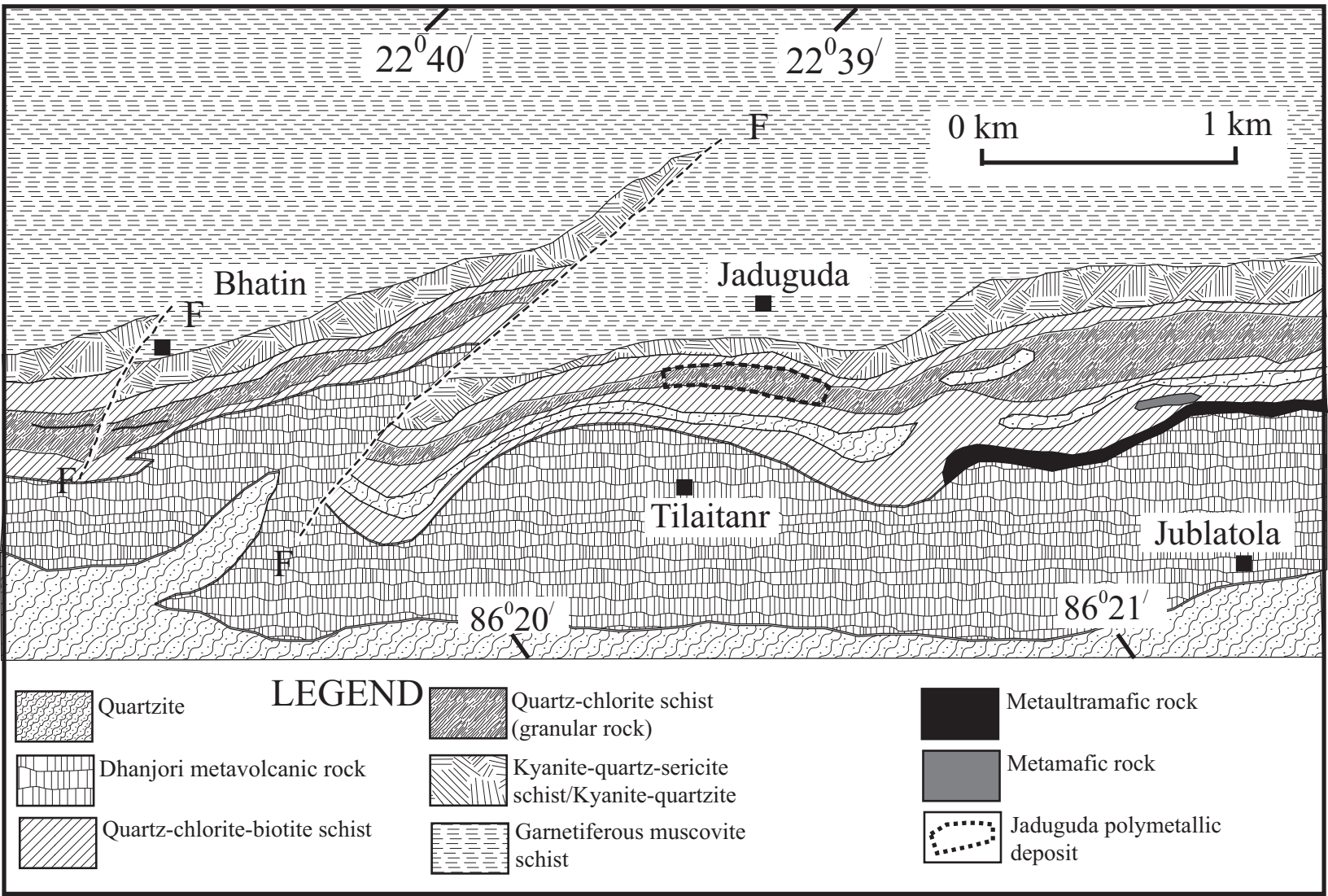
22⁰40′
22⁰39′
0 km
1 km
F
Bhatin
Jaduguda
Tilaitanr
Jublatola
86⁰20′
86⁰21′
LEGEND
Quartzite
Dhanjori metavolcanic rock
Quartz-chlorite-biotite schist
Quartz-chlorite schist (granular rock)
Kyanite-quartz-sericite schist/Kyanite-quartzite
Garnetiferous muscovite schist
Metaultramafic rock
Metamafic rock
Jaduguda polymetallic deposit

Figure 3

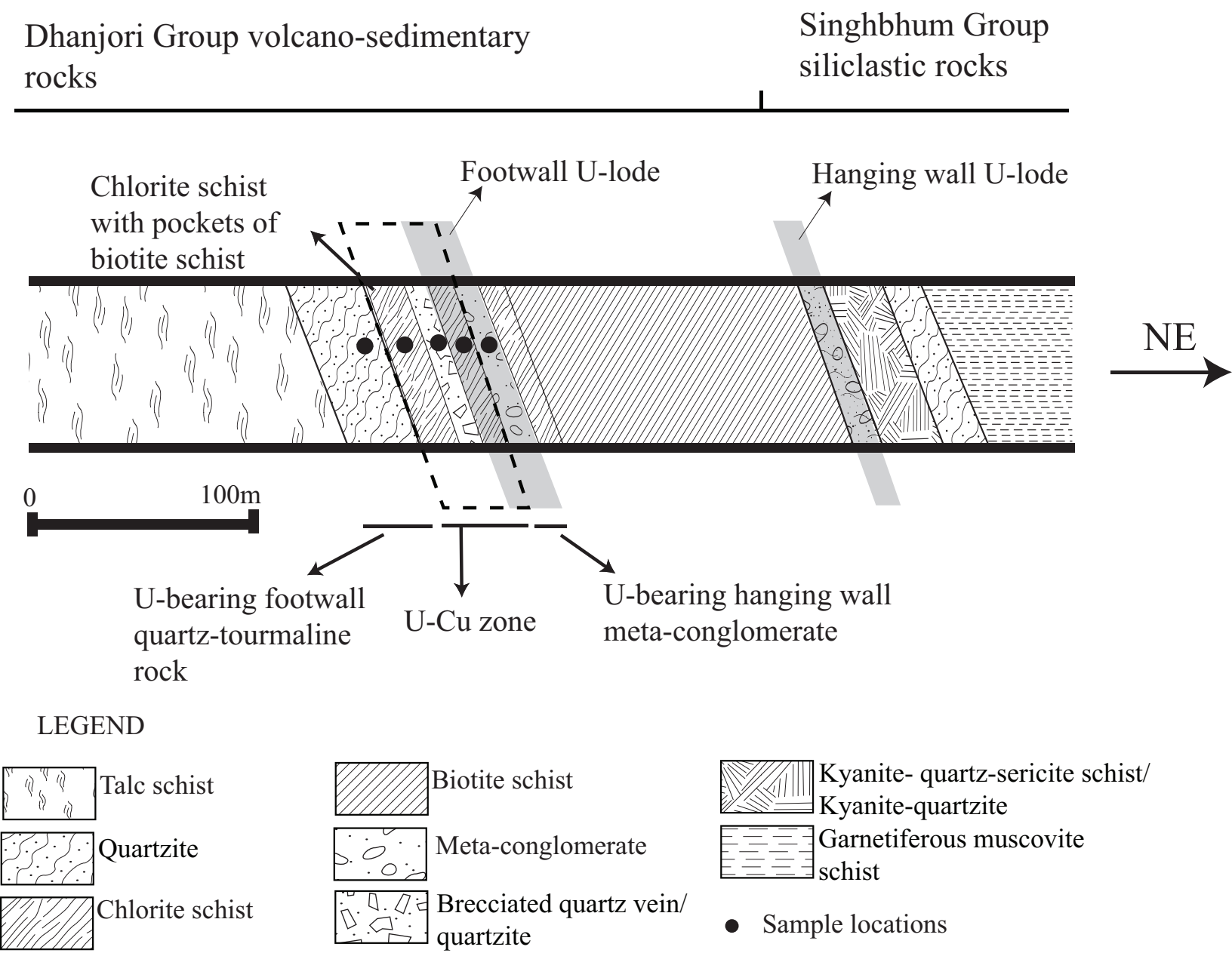
Dhanjori Group volcano-sedimentary rocks
Singhbhum Group siliclastic rocks
Chlorite schist with pockets of biotite schist
Footwall U-lode
Hanging wall U-lode
NE
0
100m
U-bearing footwall quartz-tourmaline rock
U-Cu zone
U-bearing hanging wall meta-conglomerate
LEGEND
Talc schist
Quartzite
Chlorite schist
Biotite schist
Meta-conglomerate
Brecciated quartz vein/ quartzite
Kyanite- quartz-sericite schist/ Kyanite-quartzite
Garnetiferous muscovite schist
Sample locations

Figure 4
Click here to download high resolution image

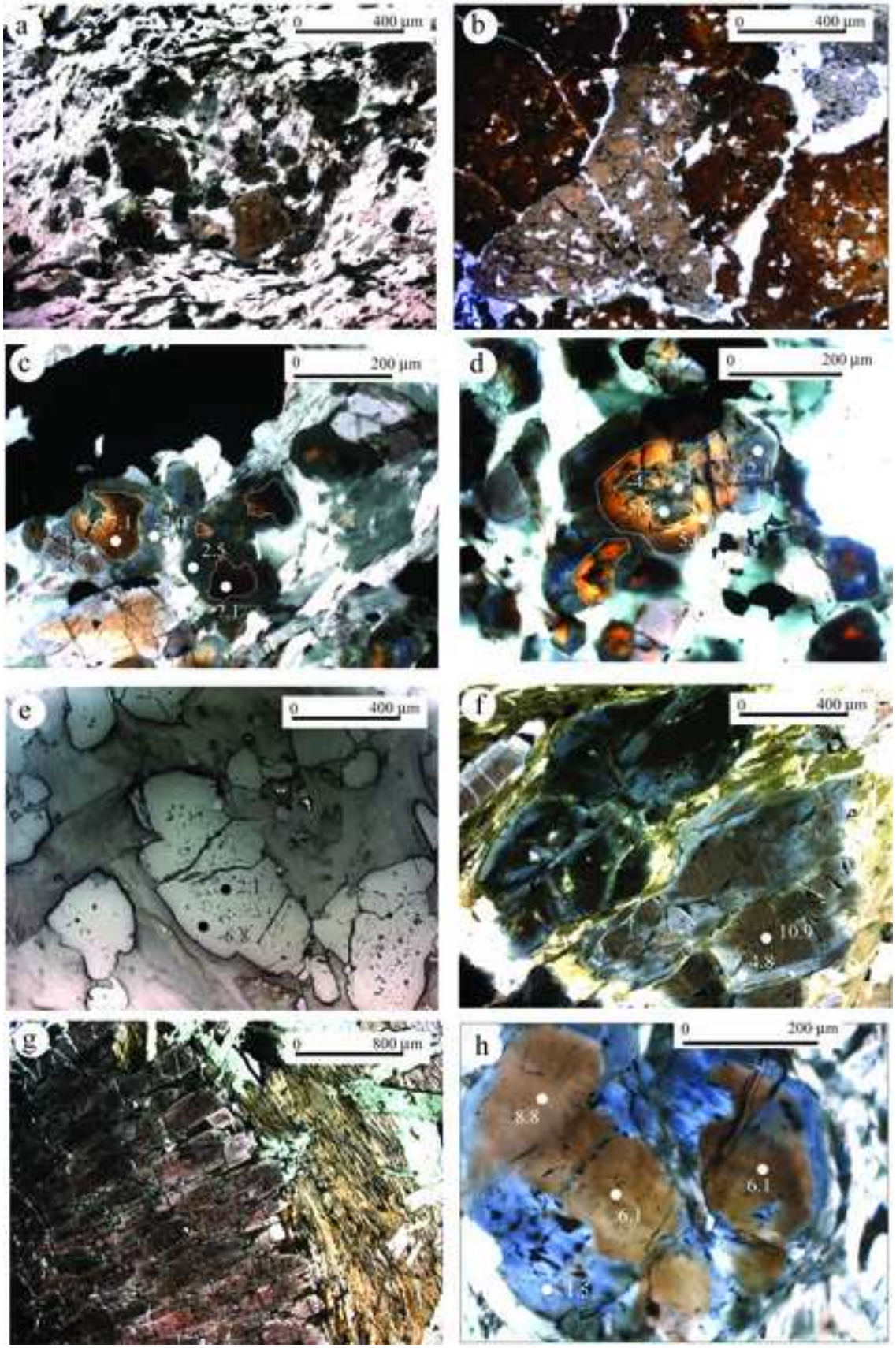

Figure 5

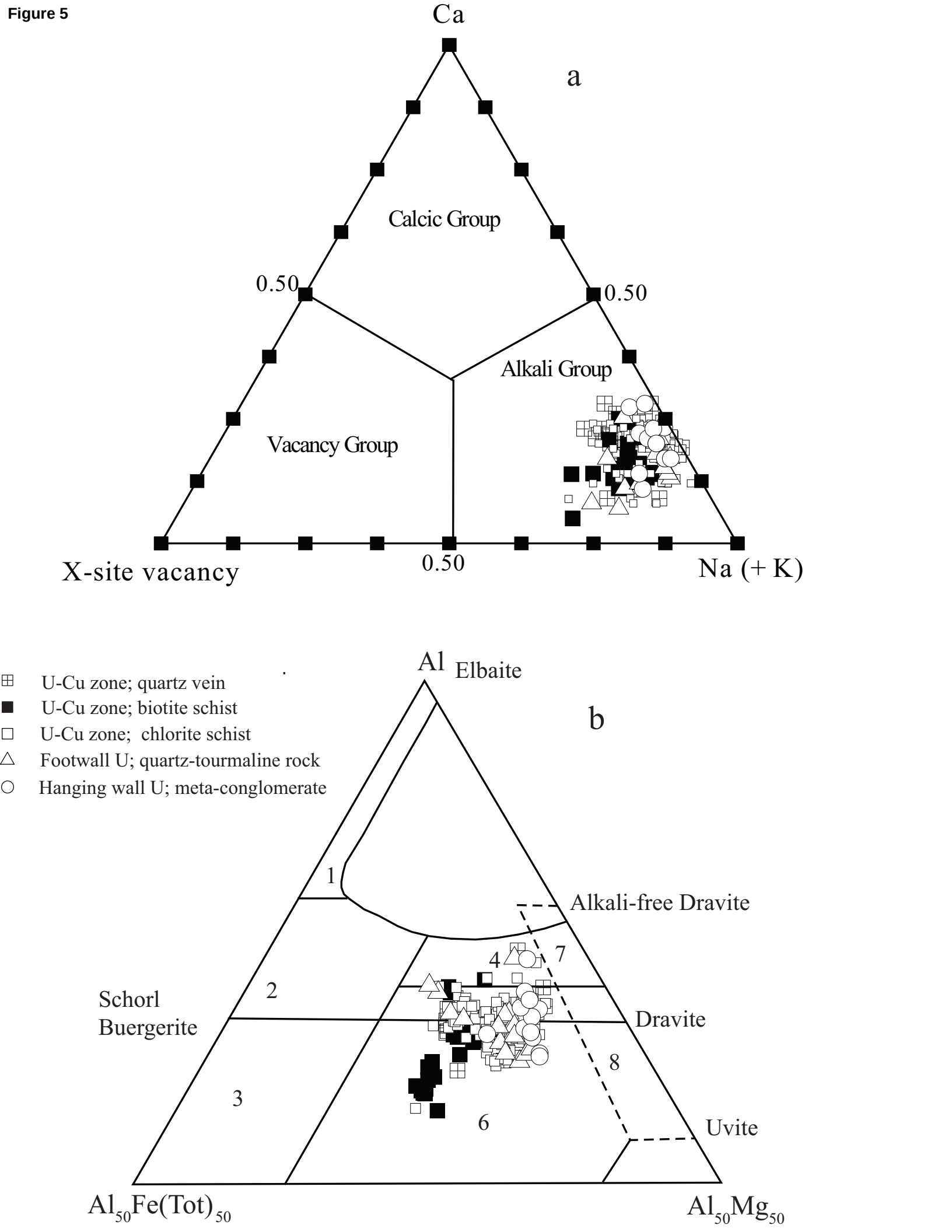
Ca
a
Calcic Group
0.50
0.50
Alkali Group
Vacancy Group
X-site vacancy
0.50
Na (+ K)
U-Cu zone; quartz vein
U-Cu zone; biotite schist
U-Cu zone; chlorite schist
Footwall U; quartz-tourmaline rock
Hanging wall U; meta-conglomerate
Al
Elbaite
b
1
Alkali-free Dravite
4
7
2
Schorl
Buergerite
Dravite
8
3
6
Uvite
$Al_{50}Fe(Tot)_{50}$
$Al_{50}Mg_{50}$

Figure 6

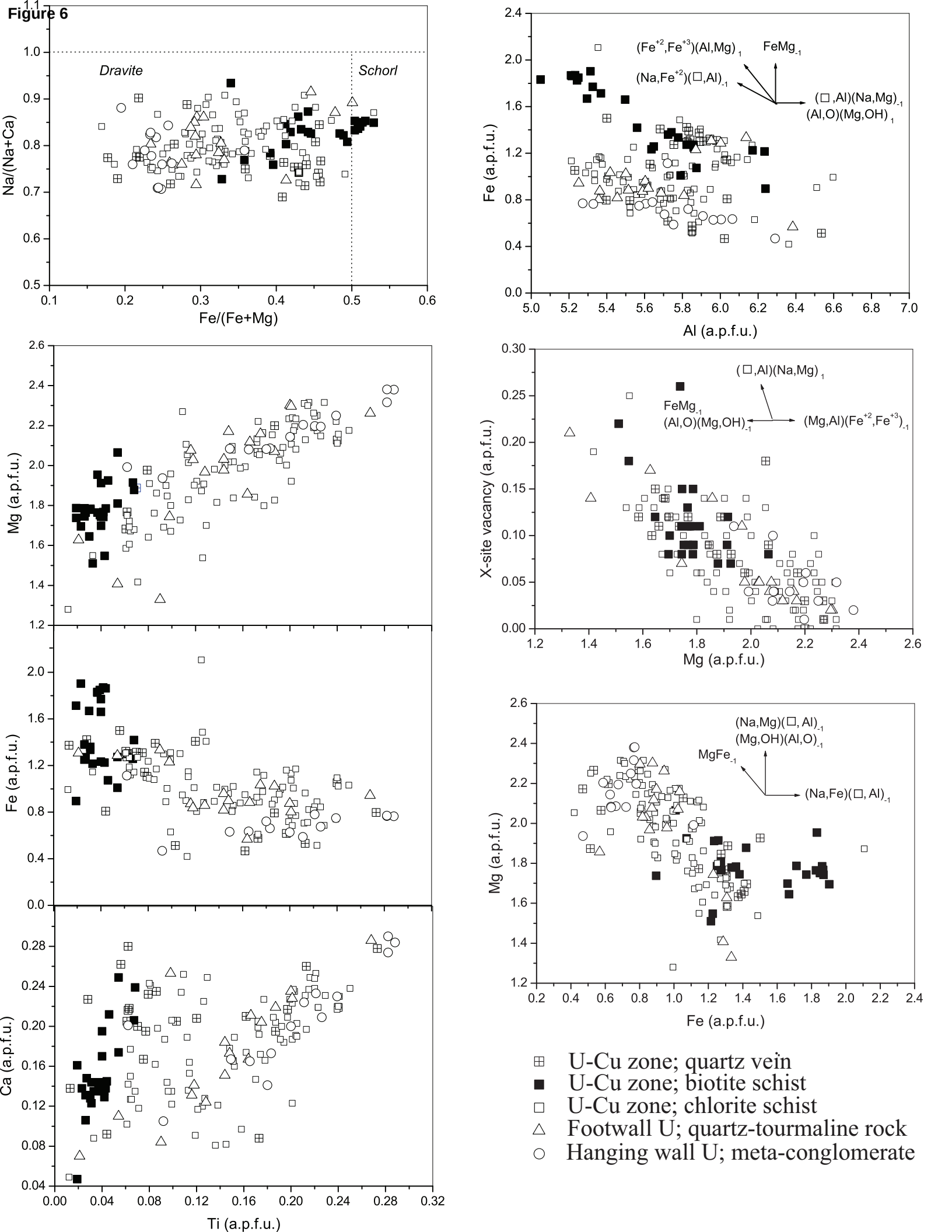
Dravite
Schorl
Na/(Na+Ca)
Fe/(Fe+Mg)
(Fe+2,Fe+3)(Al,Mg)1
FeMg-1
(Na,Fe+2)(□,Al)-1
(□,Al)(Na,Mg)-1
(Al,O)(Mg,OH)1
Fe (a.p.f.u.)
Al (a.p.f.u.)
(□,Al)(Na,Mg)1
FeMg-1
(Al,O)(Mg,OH)-1
(Mg,Al)(Fe+2,Fe+3)-1
X-site vacancy (a.p.f.u.)
Mg (a.p.f.u.)
(Na,Mg)(□,Al)-1
(Mg,OH)(Al,O)-1
MgFe-1
(Na,Fe)(□,Al)-1
Mg (a.p.f.u.)
Fe (a.p.f.u.)
Fe (a.p.f.u.)
Ca (a.p.f.u.)
Ti (a.p.f.u.)
U-Cu zone; quartz vein
U-Cu zone; biotite schist
U-Cu zone; chlorite schist
Footwall U; quartz-tourmaline rock
Hanging wall U; meta-conglomerate

Figure 7

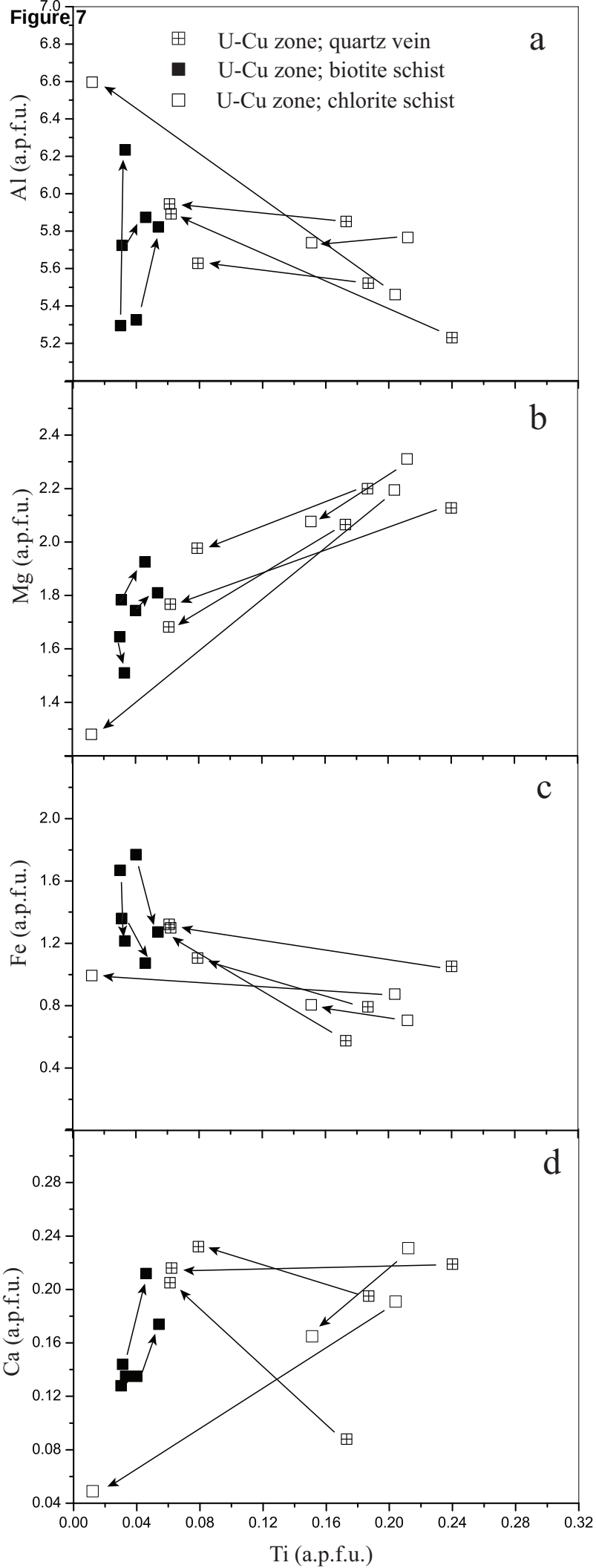
U-Cu zone; quartz vein
U-Cu zone; biotite schist
U-Cu zone; chlorite schist
a
b
c
d
Al (a.p.f.u.)
Mg (a.p.f.u.)
Fe (a.p.f.u.)
Ca (a.p.f.u.)
Ti (a.p.f.u.)

Figure 8

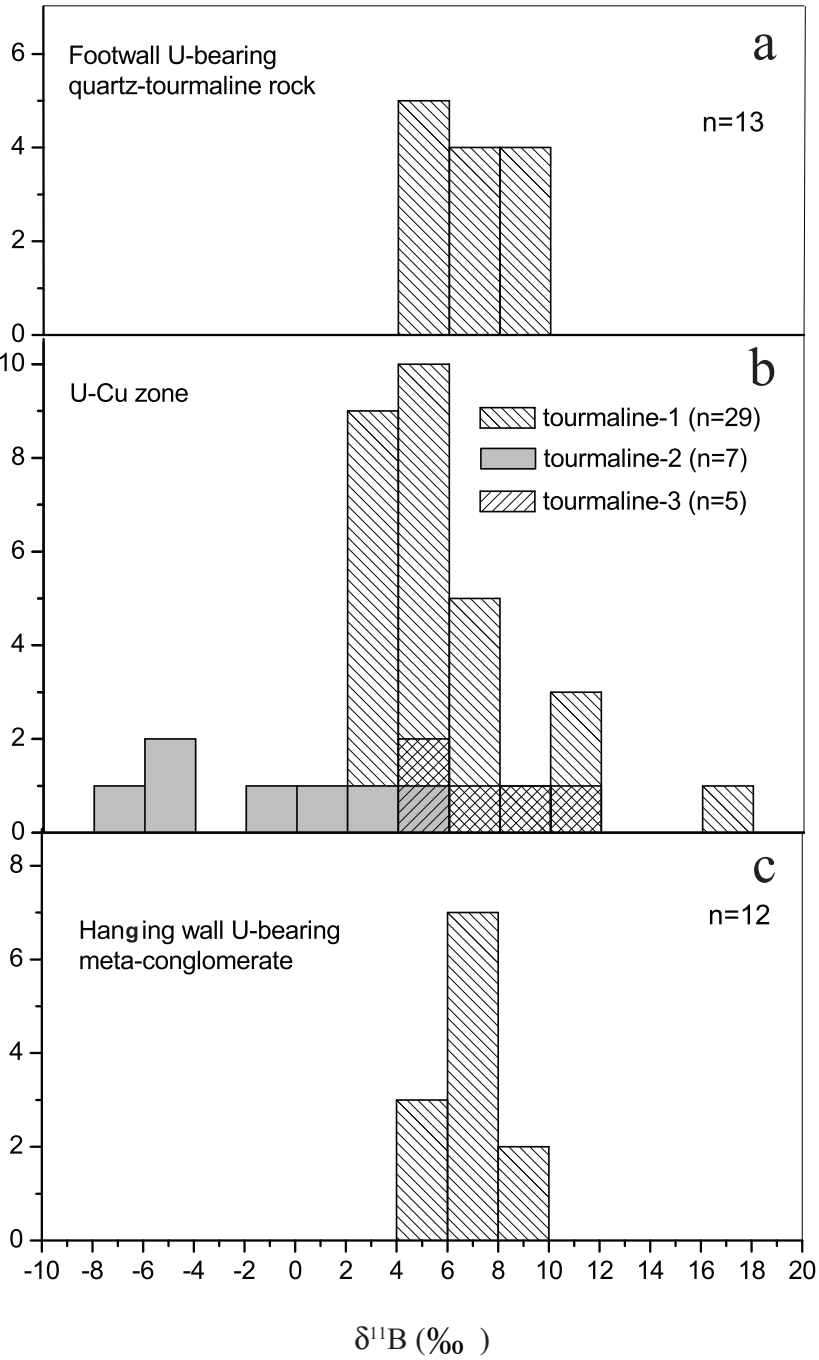
a
Footwall U-bearing
quartz-tourmaline rock
n=13
b
U-Cu zone
tourmaline-1 (n=29)
tourmaline-2 (n=7)
tourmaline-3 (n=5)
c
n=12
Hanging wall U-bearing
meta-conglomerate
δ11B (‰)

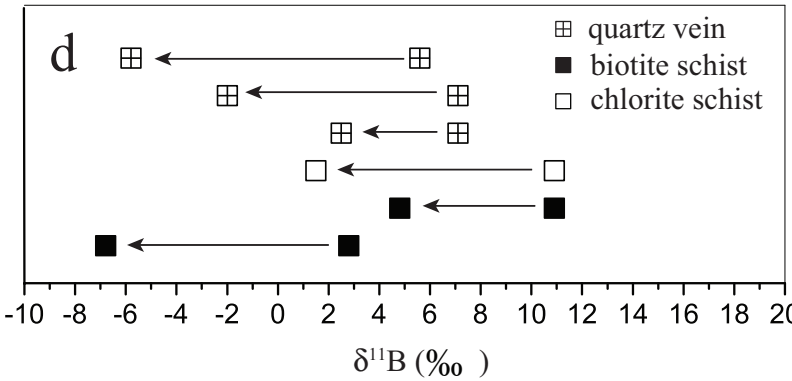
d
quartz vein
biotite schist
chlorite schist
δ11B (‰)

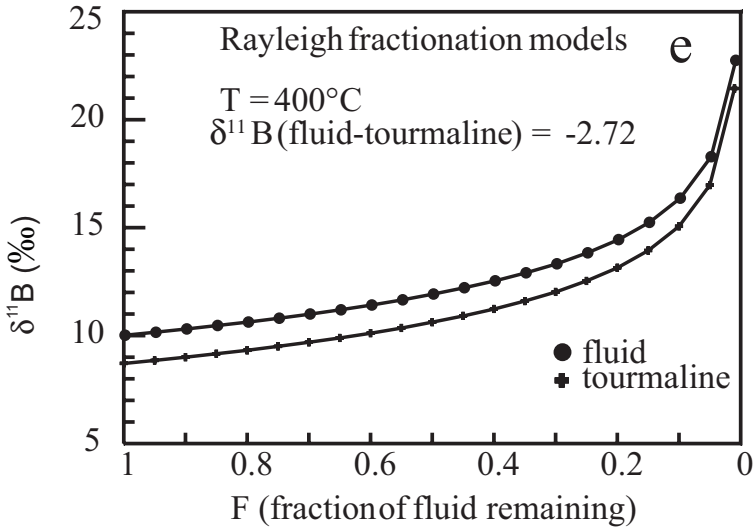
Rayleigh fractionation models
e
T = 400°C
δ11B (fluid-tourmaline) = -2.72
δ11B (‰)
fluid
tourmaline
F (fraction of fluid remaining)

Table 1
Click here to download Table: Table 1.docx

Table 1

Tourmaline Reference	Certified $^{11}B/^{10}B$ values	Reference	Maximum individual uncertainty in ‰ (1 SD)	Repeatability (in ‰ from multiple analysis of each reference material; (standard deviation/mean) x 1000	
				1st session	2nd session
Schorl	3.993	HS #112566 ; Dyar et al., (2001)	± 0.4	± 1.0 (n=9)	± 0.4 (n=6)
Dravite	4.017	HS #108796; Dyar et al., (2001)	± 0.4	± 1.3 (n=8)	± 0.8 (n=7)
Elbaite	4.001	HS #98144; Dyar et al., (2001)	± 0.4	± 1.3 (n=8)	± 0.5 (n=4)
B4	4.0078	Tonarini et al., (2003)	± 0.4	± 1.6 (n=8)	± 0.7 (n=4)
			Overall repeatability	± 1.8	± 1.5

Table 2

Click here to download Table: Table 2.docx

Table 2

Sample position	Footwall quartz tourmaline rock								Hanging wall meta-conglomerate							Ore zone quartz vein					
	73	74	75	76	79	82	84	87	54	55	64	65	67	68	70	33	34	35	36	45	46
SiO_2	37.23	38.13	36.64	35.63	37.18	36.77	37.92	36.31	34.85	36.70	36.76	35.66	36.95	36.80	36.77	34.76	36.88	36.73	36.45	37.31	36.47
TiO_2	0.94	0.44	2.10	0.17	1.59	1.48	1.16	1.34	1.65	0.76	1.20	0.48	1.34	1.90	1.62	0.55	0.60	1.46	0.62	1.37	0.49
Al_2O_3	29.66	31.10	26.22	29.59	27.15	27.74	28.86	33.28	28.66	32.82	30.76	28.40	31.55	28.27	30.80	29.33	30.92	27.56	28.18	29.63	30.72
MgO	8.20	5.77	8.93	6.40	9.22	8.26	8.05	7.66	8.68	7.99	8.44	7.82	8.56	9.03	8.76	7.50	6.48	8.69	7.83	8.27	6.88
MnO	0.00	0.02	0.04	0.00	0.00	0.01	0.00	0.01	0.00	0.02	0.00	0.00	0.03	0.00	0.01	0.00	0.01	0.02	0.00	0.02	0.00
FeO	6.03	9.39	6.63	9.16	6.25	7.27	6.96	4.17	4.12	3.45	4.56	7.79	4.65	5.35	4.56	9.29	9.54	5.58	7.81	4.10	9.63
Cr_2O_3	0.18	0.04	0.33	0.08	0.23	0.27	0.55	0.93	2.32	1.89	0.34	0.14	0.23	0.30	0.20	0.13	0.02	0.39	0.26	0.63	0.03
CaO	0.79	0.63	1.57	0.39	1.31	1.21	1.04	0.96	1.23	0.60	0.94	1.10	0.95	1.29	1.14	1.11	0.95	1.07	1.28	0.49	1.17
Na_2O	2.48	2.34	2.19	2.29	2.28	2.25	2.37	2.16	2.15	2.47	2.43	2.28	2.51	2.25	2.37	1.98	2.22	2.41	2.12	2.50	2.03
K_2O	0.05	0.04	0.07	0.04	0.03	0.04	0.05	0.03	0.04	0.03	0.04	0.03	0.04	0.05	0.03	0.16	0.03	0.04	0.03	0.03	0.02
F	0.28	0.15	0.43	0.26	0.36	0.32	0.34	0.02	0.59	0.20	0.27	0.55	0.30	0.40	0.28	0.38	0.32	0.26	0.42	0.14	0.39
Cl	0.02	0.01	0.01	0.01	0.00	0.02	0.01	0.00	0.02	0.01	0.01	0.02	0.00	0.00	0.01	0.02	0.01	0.01	0.01	0.01	0.02
Sum	85.84	88.06	85.16	84.01	85.59	85.63	87.31	86.86	84.31	86.96	85.76	84.26	87.09	85.64	86.55	85.20	88.00	84.21	85.01	84.50	87.84
Si (a.p.f.u)	6.185	6.243	6.225	6.081	6.230	6.184	6.246	5.908	5.934	5.966	6.086	6.094	6.024	6.152	6.039	5.872	6.048	6.243	6.175	6.249	5.986
Al(T)	0.000	0.000	0.000	0.000	0.000	0.000	0.000	0.092	0.066	0.034	0.000	0.000	0.000	0.000	0.000	0.128	0.000	0.000	0.000	0.000	0.014
Al(Z)	5.808	6.000	5.252	5.953	5.363	5.500	5.603	6.000	5.686	6.000	6.000	5.721	6.000	5.571	5.963	5.712	5.980	5.522	5.628	5.851	5.931
Al(Y)	0.000	0.003	0.000	0.000	0.000	0.000	0.000	0.291	0.000	0.256	0.005	0.000	0.064	0.000	0.000	0.000	0.000	0.000	0.000	0.000	0.000
Ti	0.118	0.054	0.268	0.021	0.200	0.187	0.144	0.164	0.211	0.092	0.149	0.062	0.165	0.239	0.200	0.070	0.075	0.187	0.079	0.173	0.061
Mg	2.029	1.407	2.262	1.627	2.302	2.070	1.977	1.857	2.204	1.937	2.084	1.992	2.080	2.250	2.144	1.888	1.584	2.200	1.977	2.065	1.682
Mn	0.000	0.002	0.005	0.000	0.000	0.001	0.000	0.001	0.000	0.003	0.000	0.000	0.004	0.000	0.001	0.000	0.002	0.003	0.000	0.003	0.000
Fe	0.837	1.286	0.943	1.307	0.875	1.023	0.959	0.567	0.587	0.469	0.632	1.113	0.634	0.748	0.627	1.313	1.309	0.793	1.106	0.575	1.322
Cr	0.023	0.006	0.045	0.011	0.030	0.036	0.072	0.120	0.312	0.243	0.045	0.019	0.030	0.039	0.026	0.018	0.003	0.052	0.035	0.083	0.004
Ca	0.141	0.110	0.286	0.070	0.235	0.219	0.184	0.167	0.224	0.105	0.167	0.201	0.165	0.230	0.200	0.200	0.167	0.195	0.232	0.088	0.205
Na	0.798	0.743	0.722	0.756	0.742	0.733	0.756	0.683	0.709	0.779	0.781	0.755	0.794	0.730	0.753	0.648	0.706	0.795	0.697	0.810	0.646
K	0.011	0.009	0.016	0.008	0.007	0.009	0.010	0.006	0.008	0.007	0.008	0.005	0.007	0.011	0.007	0.035	0.006	0.008	0.007	0.006	0.003
vacancies	0.049	0.138	0.000	0.165	0.016	0.040	0.050	0.144	0.058	0.109	0.043	0.038	0.033	0.029	0.039	0.117	0.120	0.002	0.064	0.095	0.145
$^{11}B/^{10}B$	4.068	4.074	4.077	4.076	4.063	4.063	4.068	4.062	4.072	4.074	4.077	4.071	4.068	4.082	4.069	4.066	4.055	4.072	4.035	4.072	4.054
1σ uncertainty (‰)	0.38	0.35	0.34	0.32	0.37	0.38	0.36	0.29	0.37	0.35	0.35	0.36	0.38	0.51	0.45	0.37	0.37	0.37	0.36	0.41	0.39
$\delta\ ^{11}B$	6.0	7.6	8.3	8.6	4.8	4.8	6.1	4.5	7.1	7.6	8.3	6.8	6.1	9.6	6.3	5.6	2.8	7.1	-2.0	7.1	2.5

Table 2 continued

Sample position	Ore zone-quartz vein				Ore zone-biotite schist							Ore zone-chlorite schist							
	31	32	33	34	7	8	11	12	25	27	28	114	115	119	120	16	18	43	45
SiO_2	35.54	36.77	34.76	36.88	34.60	36.96	37.14	36.75	35.86	36.46	36.49	36.48	36.58	36.96	36.97	36.72	37.90	36.56	36.11
TiO_2	1.66	0.45	0.55	0.60	0.23	0.27	0.25	0.37	0.32	0.35	0.31	1.72	1.18	0.53	1.63	1.61	0.10	0.65	1.76
Al_2O_3	29.05	27.56	29.33	30.92	26.44	32.59	29.56	30.16	28.90	26.47	26.61	29.79	28.73	31.26	30.50	27.50	34.71	30.02	29.44
MgO	8.90	7.78	7.50	6.48	6.50	6.25	7.29	7.82	7.75	7.17	7.03	9.44	8.23	6.82	9.24	8.75	5.33	7.75	8.96
MnO	0.00	0.01	0.00	0.01	0.01	0.06	0.00	0.06	0.00	0.03	0.01	0.00	0.00	0.01	0.02	0.01	0.02	0.03	0.00
FeO	3.72	10.80	9.29	9.54	11.75	8.95	9.90	7.77	8.92	13.32	13.21	5.14	5.68	8.13	5.29	6.21	7.38	7.89	3.65
Cr_2O_3	0.48	0.02	0.13	0.02	3.61	0.02	0.00	0.01	1.89	0.00	0.02	0.11	0.24	0.06	0.12	0.60	0.04	0.14	0.53
CaO	1.42	1.47	1.11	0.95	0.70	0.78	0.82	1.20	1.10	0.81	0.75	1.31	0.91	0.72	1.31	1.06	0.28	1.36	1.21
Na_2O	2.11	2.03	1.98	2.22	2.25	2.04	2.28	2.21	2.21	2.36	2.35	2.22	2.43	2.29	2.12	2.38	1.55	2.05	2.12
K_2O	0.06	0.03	0.16	0.03	0.05	0.04	0.20	0.03	0.02	0.04	0.05	0.08	0.03	0.01	0.03	0.04	0.03	0.02	0.04
F	0.35	0.53	0.38	0.32	0.00	0.00	0.11	0.31	0.02	0.09	0.00	0.39	0.31	0.20	0.47	0.32	0.00	0.38	0.40
Cl	0.01	0.00	0.02	0.01	0.01	0.01	0.03	0.00	0.02	0.00	0.01	0.01	0.01	0.01	0.01	0.00	0.02	0.00	0.00
Sum	83.29	87.43	85.20	88.00	86.14	87.96	87.58	86.69	87.00	87.10	86.82	86.70	84.32	86.99	87.71	85.20	87.35	86.85	84.22
Si (a.p.f.u)	6.073	6.112	5.872	6.048	5.876	5.997	6.100	6.071	5.932	6.091	6.107	5.991	6.198	6.076	5.998	6.184	6.109	6.044	6.089
Al(T)	0.000	0.000	0.128	0.000	0.124	0.003	0.000	0.000	0.068	0.000	0.000	0.010	0.000	0.000	0.002	0.000	0.000	0.000	0.000
Al(Z)	5.851	5.400	5.712	5.980	5.171	6.000	5.724	5.874	5.568	5.215	5.249	5.757	5.738	6.000	5.831	5.461	6.000	5.852	5.851
Al(Y)	0.000	0.000	0.000	0.000	0.000	0.231	0.000	0.000	0.000	0.000	0.000	0.000	0.000	0.059	0.000	0.000	0.597	0.000	0.000
Ti	0.213	0.056	0.070	0.075	0.030	0.033	0.031	0.046	0.040	0.044	0.039	0.212	0.151	0.065	0.199	0.204	0.012	0.081	0.223
Mg	2.266	1.927	1.888	1.584	1.645	1.510	1.784	1.925	1.912	1.785	1.752	2.311	2.077	1.672	2.234	2.195	1.280	1.910	2.251
Mn	0.000	0.001	0.000	0.002	0.002	0.009	0.000	0.008	0.000	0.004	0.001	0.000	0.000	0.001	0.003	0.002	0.003	0.004	0.000
Fe	0.532	1.501	1.313	1.309	1.669	1.215	1.360	1.073	1.234	1.862	1.849	0.706	0.805	1.119	0.718	0.874	0.994	1.090	0.515
Cr	0.065	0.003	0.018	0.003	0.484	0.003	0.000	0.002	0.247	0.001	0.003	0.015	0.031	0.008	0.016	0.080	0.004	0.018	0.071
Ca	0.260	0.262	0.200	0.167	0.128	0.135	0.144	0.212	0.195	0.145	0.135	0.231	0.165	0.127	0.227	0.191	0.049	0.241	0.219
Na	0.700	0.654	0.648	0.706	0.740	0.640	0.725	0.707	0.710	0.766	0.762	0.706	0.799	0.731	0.668	0.777	0.485	0.656	0.694
K	0.012	0.006	0.035	0.006	0.011	0.007	0.043	0.007	0.004	0.009	0.011	0.017	0.006	0.003	0.005	0.008	0.006	0.004	0.008
X-site vacancies	0.028	0.078	0.117	0.120	0.121	0.217	0.088	0.074	0.091	0.081	0.093	0.045	0.030	0.140	0.100	0.023	0.460	0.099	0.079
$^{11}B/^{10}B$	4.020	4.053	4.066	4.055	4.088	4.063	4.055	4.016	4.089	4.074	4.060	4.058	4.063	4.062	4.060	4.079	4.050	4.063	4.062
1σ uncertainty (‰)	0.37	0.39	0.37	0.37	0.45	0.44	0.41	0.38	0.39	0.48	0.37	0.38	0.32	0.32	0.32	0.35	0.38	0.34	0.31
$\delta^{11}B$	-5.8	2.3	5.6	2.8	10.9	4.8	2.8	-6.8	11.1	7.6	4.0	3.5	4.8	4.5	4.0	8.8	1.5	4.8	4.5